US 20200000436A1

(19) **United States**

(12) **Patent Application Publication** (10) **Pub. No.: US 2020/0000436 A1**

Mahfouz (43) **Pub. Date: Jan. 2, 2020**

(54) **METHOD AND APPARATUS FOR THREE DIMENSIONAL RECONSTRUCTION OF A JOINT USING ULTRASOUND**

(71) Applicant: **JointVue, LLC**, Knoxville, TN (US)

(72) Inventor: **Mohamed R. Mahfouz**, Knoxville, TN (US)

(73) Assignee: **JointVue, LLC**, Knoxville, TN (US)

(21) Appl. No.: **16/567,873**

(22) Filed: **Sep. 11, 2019**

Related U.S. Application Data

(63) Continuation of application No. 15/684,059, filed on Aug. 23, 2017, which is a continuation of application No. 13/758,151, filed on Feb. 4, 2013, now abandoned, which is a continuation-in-part of application No. PCT/US11/46318, filed on Aug. 2, 2011.

(60) Provisional application No. 61/470,952, filed on Apr. 1, 2011, provisional application No. 61/369,848, filed on Aug. 2, 2010.

Publication Classification

(51) **Int. Cl.**

A61B 8/08	(2006.01)
A61B 8/00	(2006.01)
G06T 17/00	(2006.01)

(52) **U.S. Cl.**

CPC ***A61B 8/5207*** (2013.01); ***A61B 8/0875*** (2013.01); *A61B 8/14* (2013.01); ***G06T 17/00*** (2013.01); ***A61B 8/466*** (2013.01)

(57) **ABSTRACT**

A method of generating a 3-D patient-specific bone model, the method comprising: (a) acquiring a plurality of raw radiofrequency ("RF") signals from an A-mode ultrasound scan of a patient's bone at a plurality of locations using an ultrasound probe that comprises a transducer array; (b) tracking the acquiring of the plurality of raw RF signals in 3-D space and generating corresponding tracking data; (c) transforming each of the plurality of raw RF signals into an envelope comprising a plurality of peaks by applying an envelope detection algorithm to each of the plurality of raw RF signals, each peak corresponding with a tissue interface echo; (d) identifying a bone echo from the tissue interface echoes of each of the plurality of raw RF signals to comprise a plurality of bone echoes by selecting the last peak having a normalized envelope amplitude above a preset threshold, wherein the envelope amplitude is normalized with respect to a maximum peak existing in the envelope; (e) determining a 2-D bone contour from the plurality of bone echoes corresponding to each location of the ultrasound probe to comprise 2-D bone contours; (f) transforming the 2-D bone contours into an integrated 3-D point cloud using the tracking data; and, (g) deforming a non-patient specific 3-D bone model corresponding to the patient's bone in correspondence with the integrated 3-D point cloud to generate a 3-D patient-specific bone model.

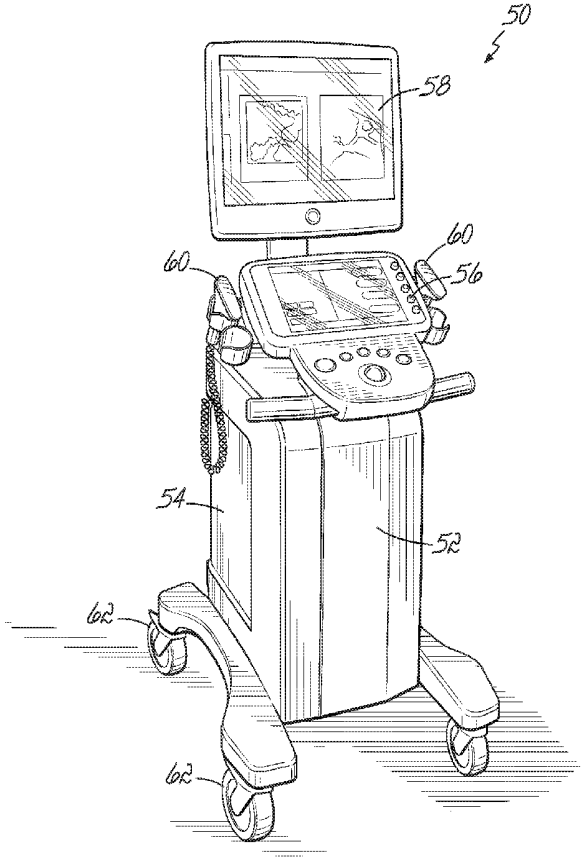

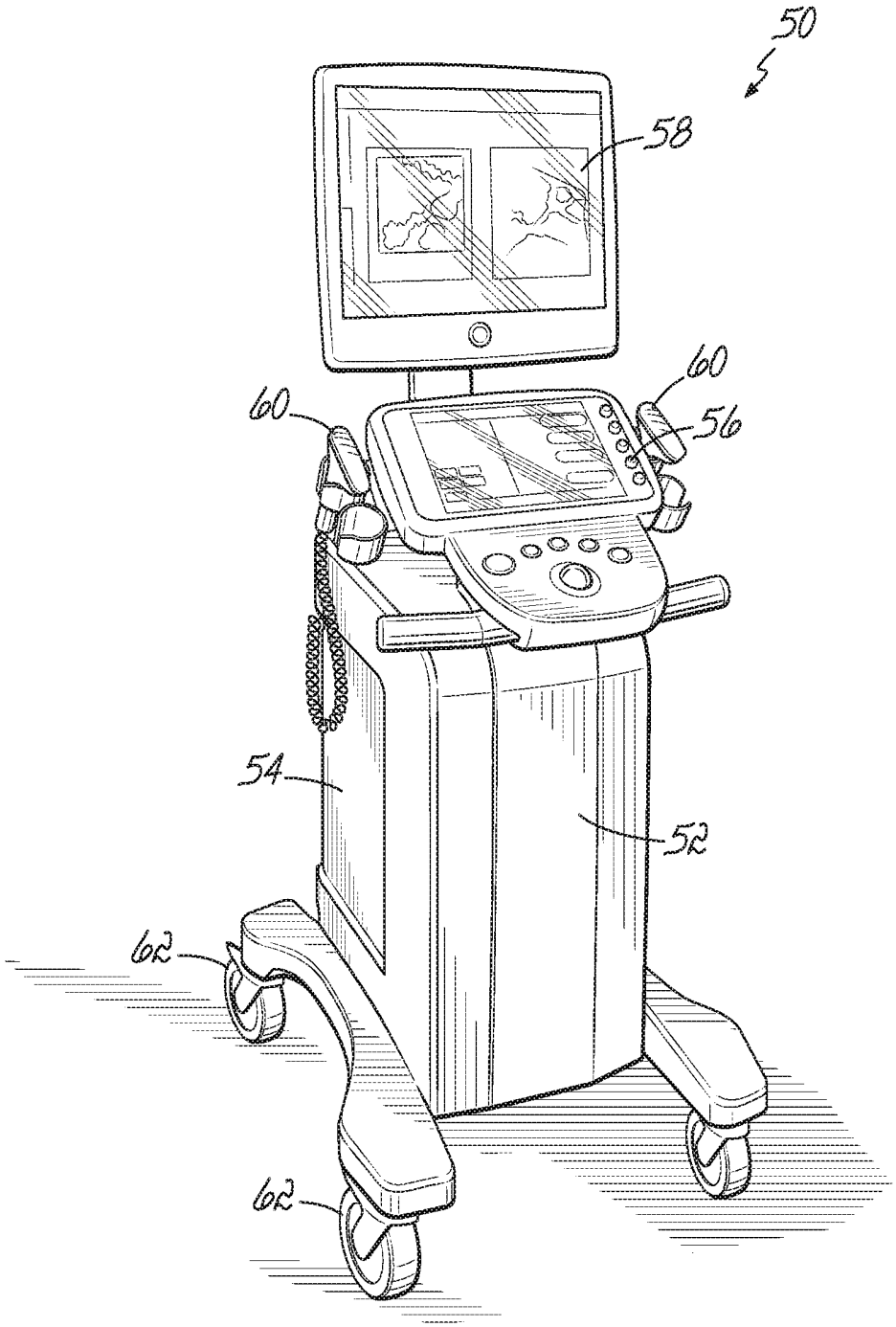

FIG. 1

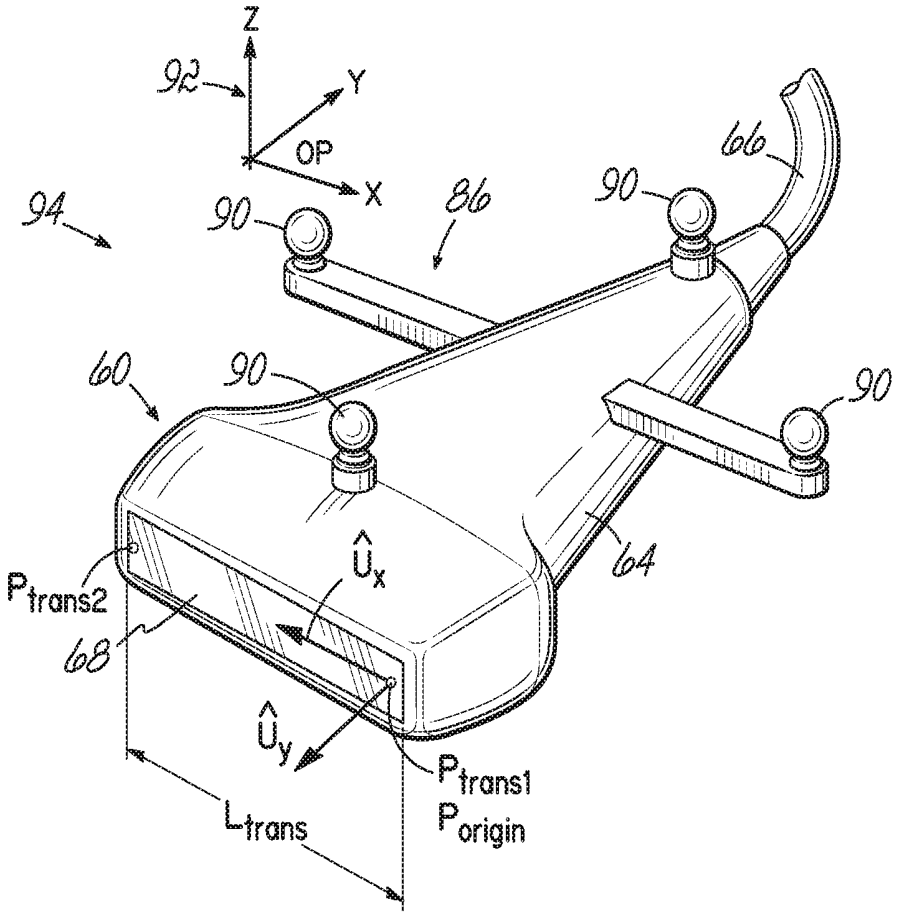
Z
92
Y
OP
X
94
90
86
90
66
60
90
90
64
$\hat{U}_x$
P_{trans2}
68
$\hat{U}_y$
P_{trans1}
P_{origin}
L_{trans}

FIG. 2

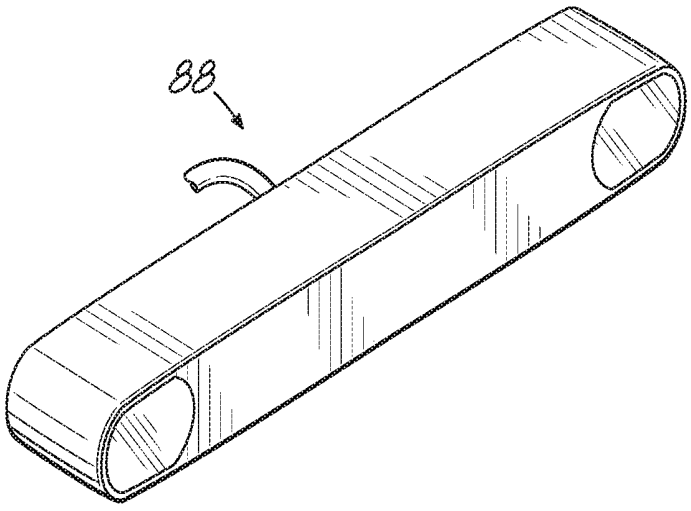
88

FIG. 2A

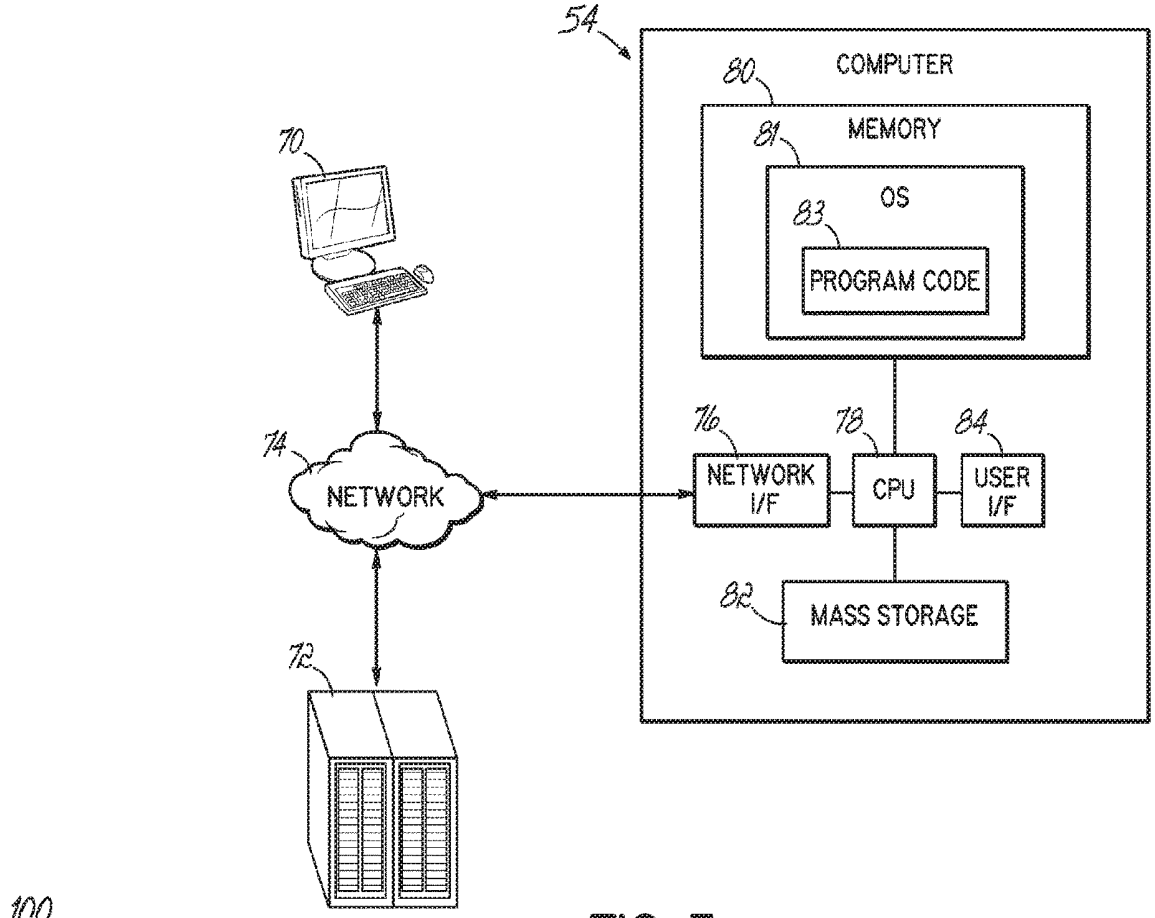
54
COMPUTER
80
MEMORY
81
OS
83
PROGRAM CODE
70
74
NETWORK
76
NETWORK I/F
78
CPU
84
USER I/F
82
MASS STORAGE
72

FIG. 3

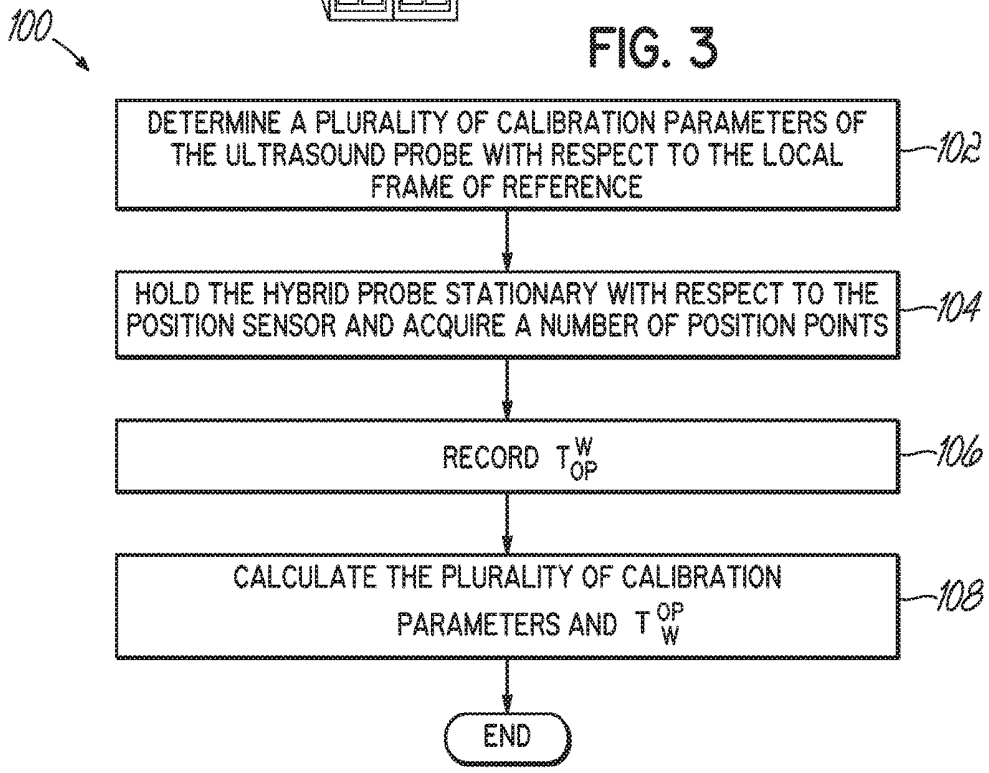
100
DETERMINE A PLURALITY OF CALIBRATION PARAMETERS OF THE ULTRASOUND PROBE WITH RESPECT TO THE LOCAL FRAME OF REFERENCE
102
HOLD THE HYBRID PROBE STATIONARY WITH RESPECT TO THE POSITION SENSOR AND ACQUIRE A NUMBER OF POSITION POINTS
104
RECORD T_{OP}^{W}
106
CALCULATE THE PLURALITY OF CALIBRATION PARAMETERS AND T_{W}^{OP}
108
END

FIG. 4

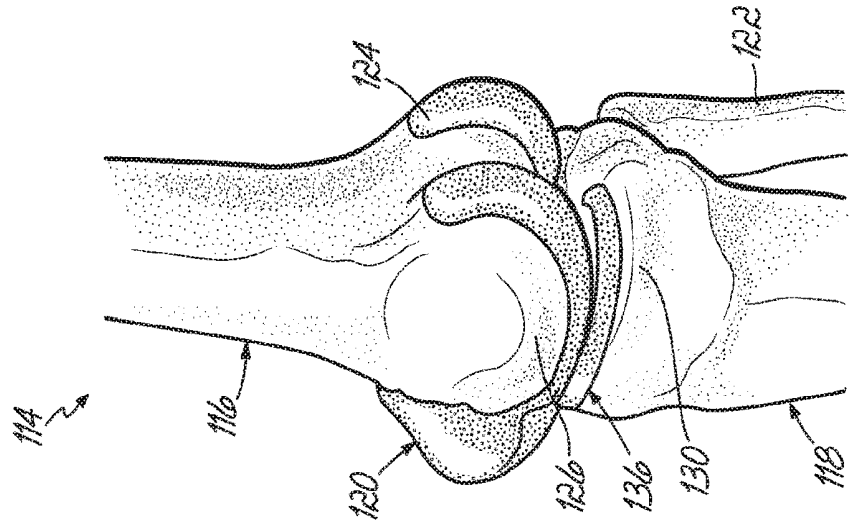

FIG. 5C

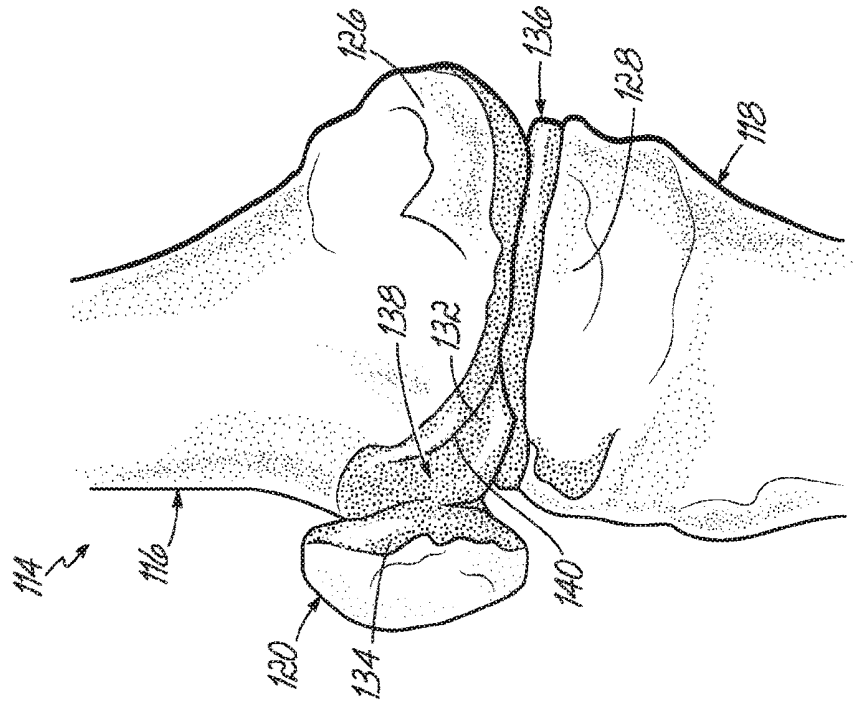

FIG. 5B

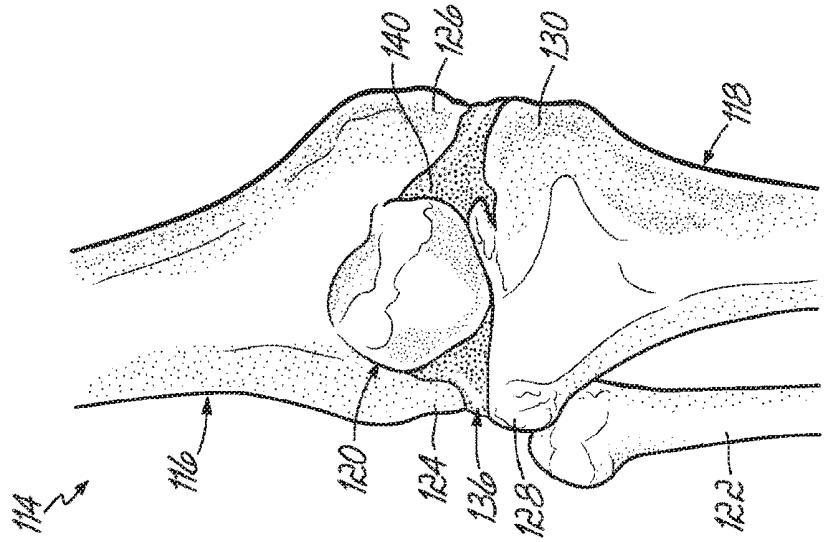

FIG. 5A

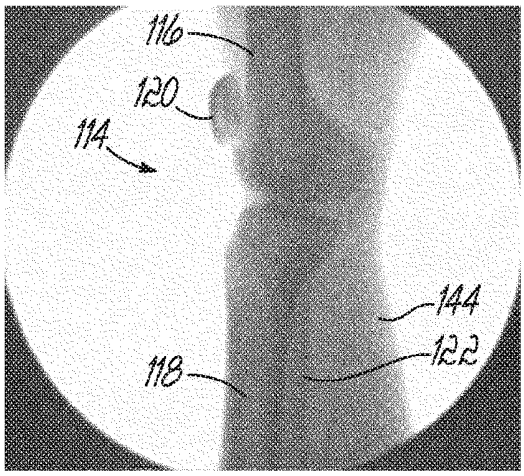

FIG. 6A

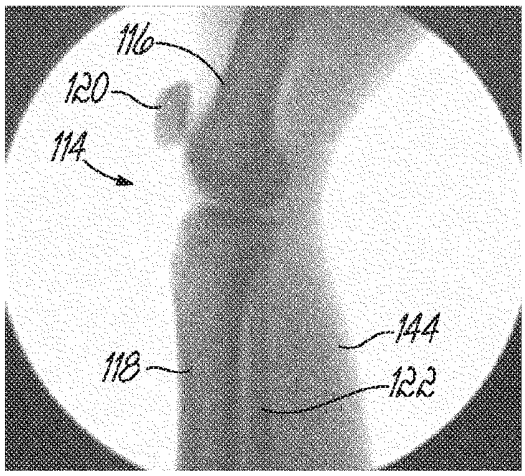

FIG. 6B

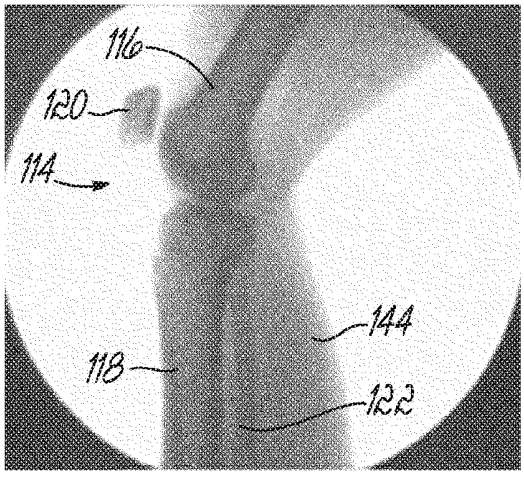

FIG. 6C

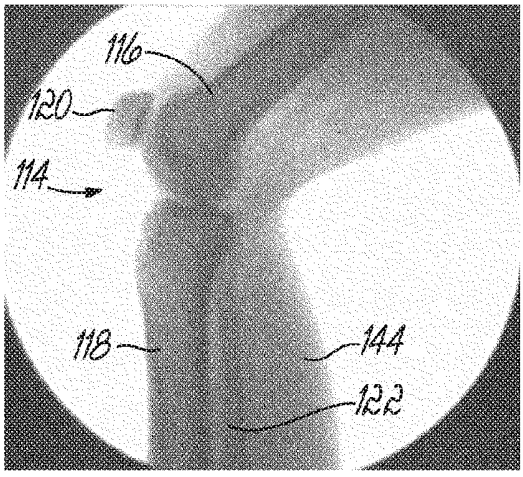

FIG. 6D

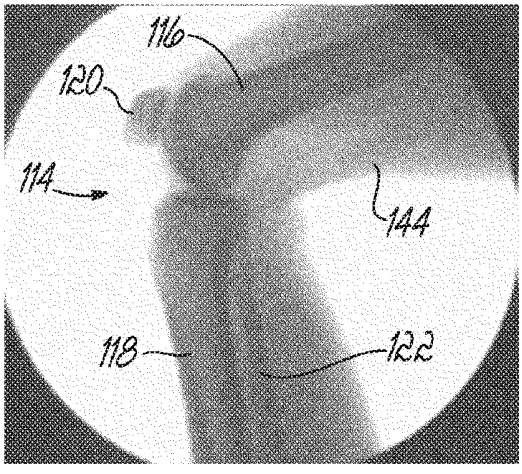

FIG. 6E

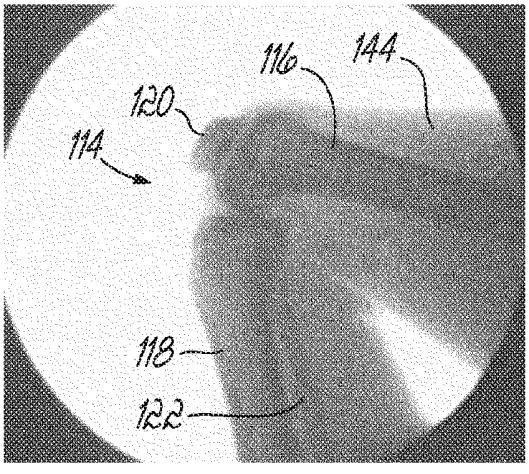

FIG. 6F

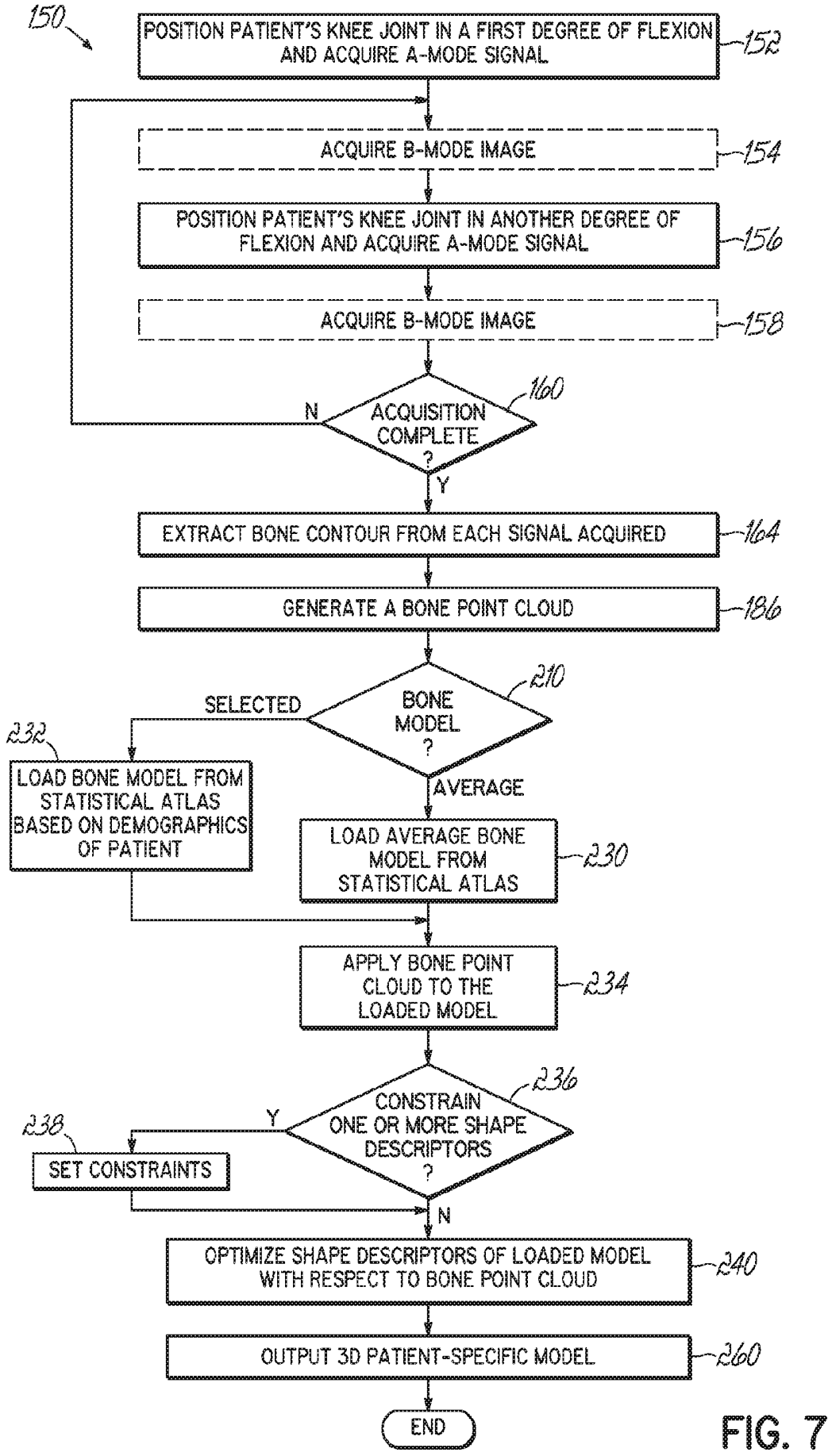
150
POSITION PATIENT'S KNEE JOINT IN A FIRST DEGREE OF FLEXION AND ACQUIRE A-MODE SIGNAL
152
ACQUIRE B-MODE IMAGE
154
POSITION PATIENT'S KNEE JOINT IN ANOTHER DEGREE OF FLEXION AND ACQUIRE A-MODE SIGNAL
156
ACQUIRE B-MODE IMAGE
158
ACQUISITION COMPLETE ?
160
N
Y
EXTRACT BONE CONTOUR FROM EACH SIGNAL ACQUIRED
164
GENERATE A BONE POINT CLOUD
186
BONE MODEL ?
210
SELECTED
AVERAGE
232
LOAD BONE MODEL FROM STATISTICAL ATLAS BASED ON DEMOGRAPHICS OF PATIENT
LOAD AVERAGE BONE MODEL FROM STATISTICAL ATLAS
230
APPLY BONE POINT CLOUD TO THE LOADED MODEL
234
CONSTRAIN ONE OR MORE SHAPE DESCRIPTORS ?
236
Y
N
238
SET CONSTRAINTS
OPTIMIZE SHAPE DESCRIPTORS OF LOADED MODEL WITH RESPECT TO BONE POINT CLOUD
240
OUTPUT 3D PATIENT-SPECIFIC MODEL
260
END

FIG. 7

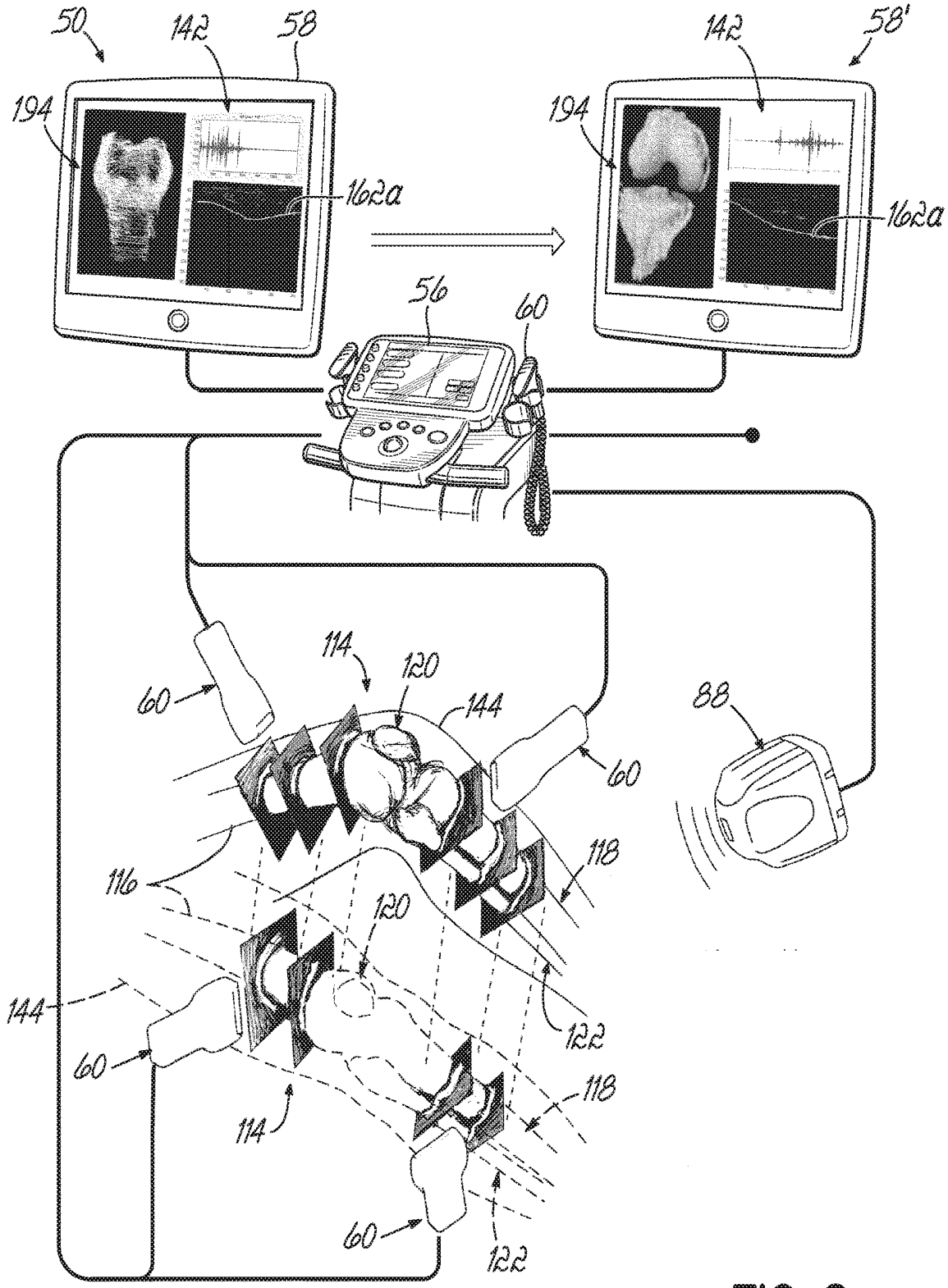
50
142
58
194
162a
142
58'
194
162a
56
60
60
114
120
144
60
88
116
118
120
144
122
60
118
114
60
122

FIG. 8

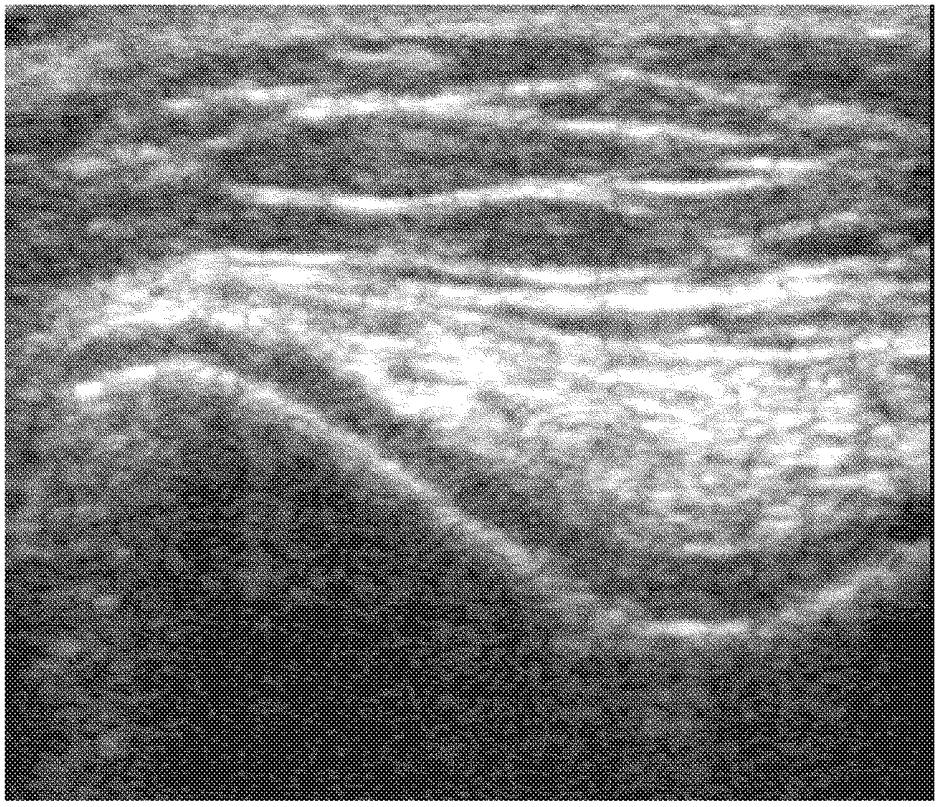

FIG. 9

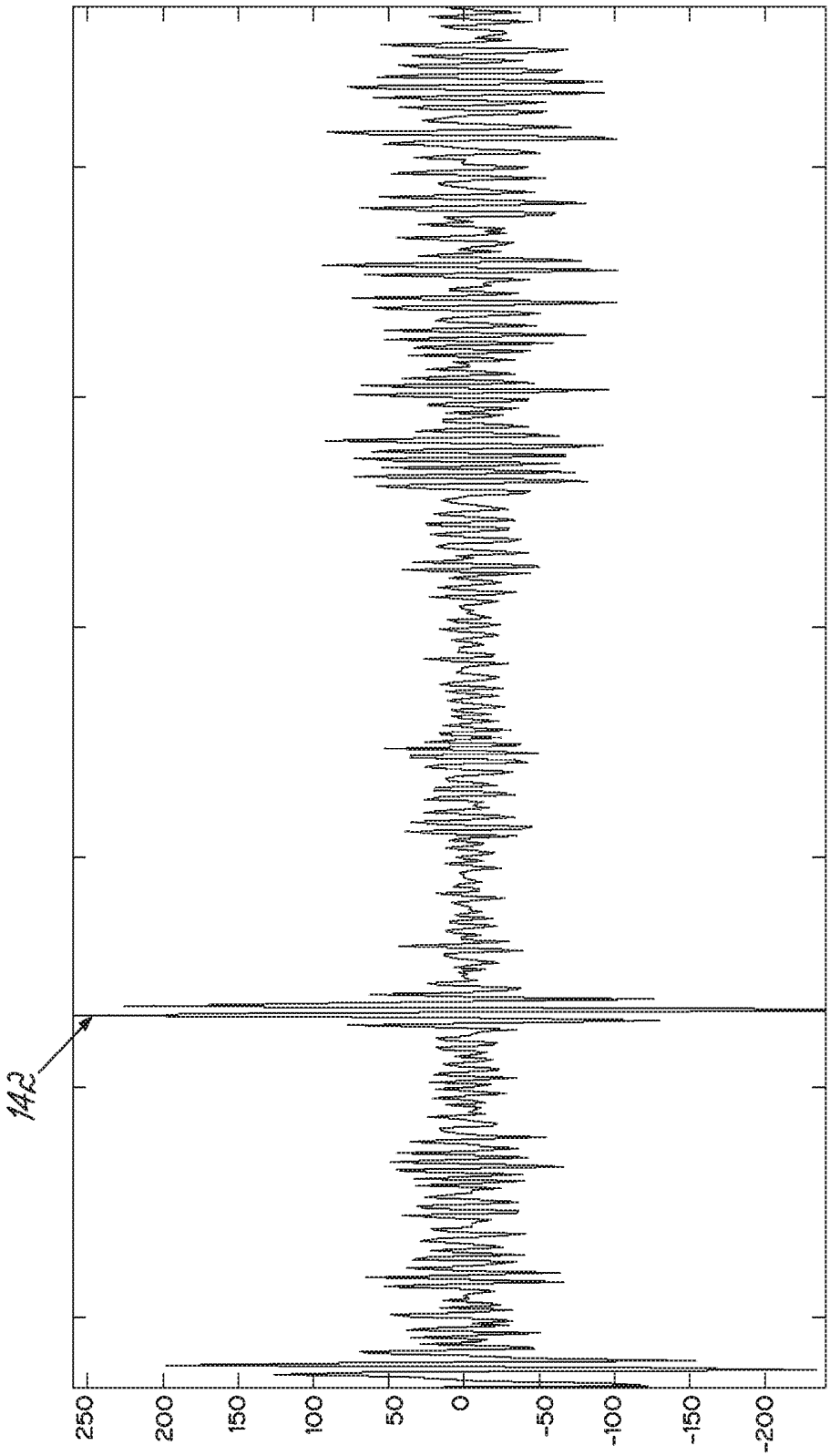

FIG. 10A

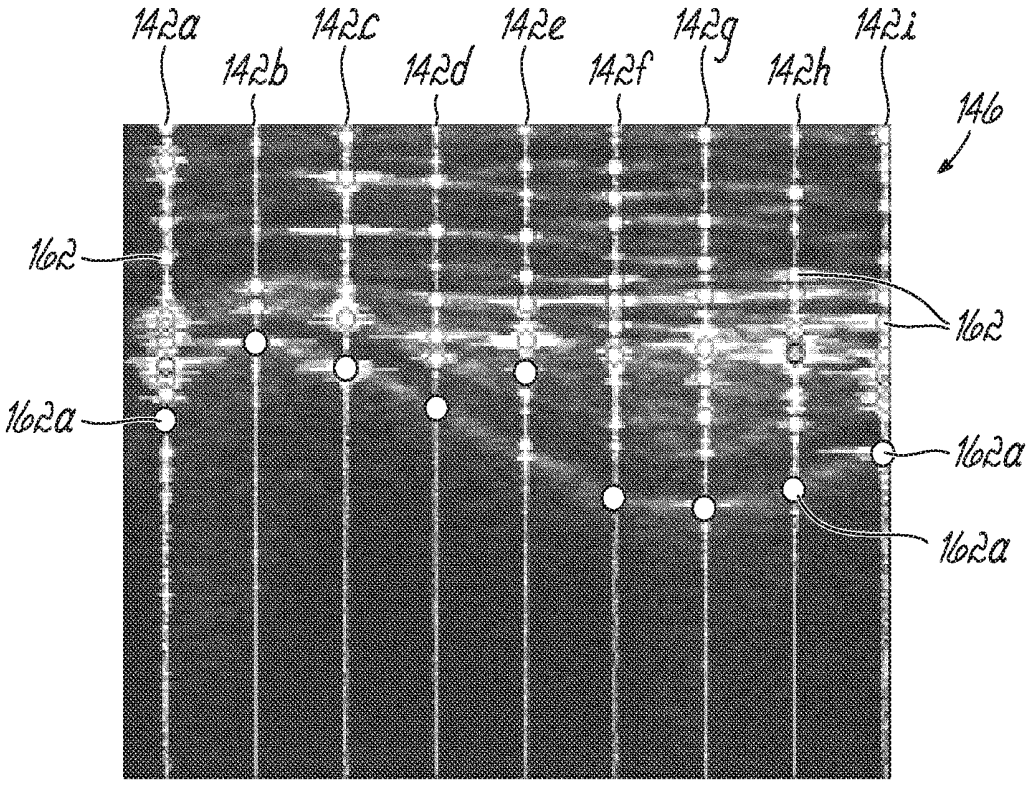

FIG. 10B

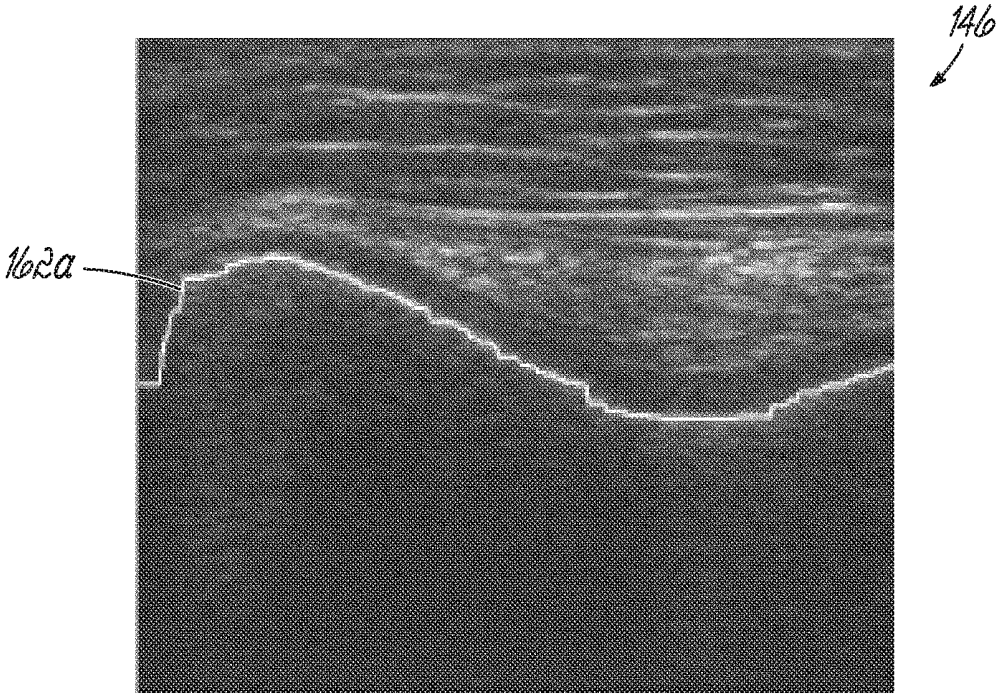

FIG. 10C

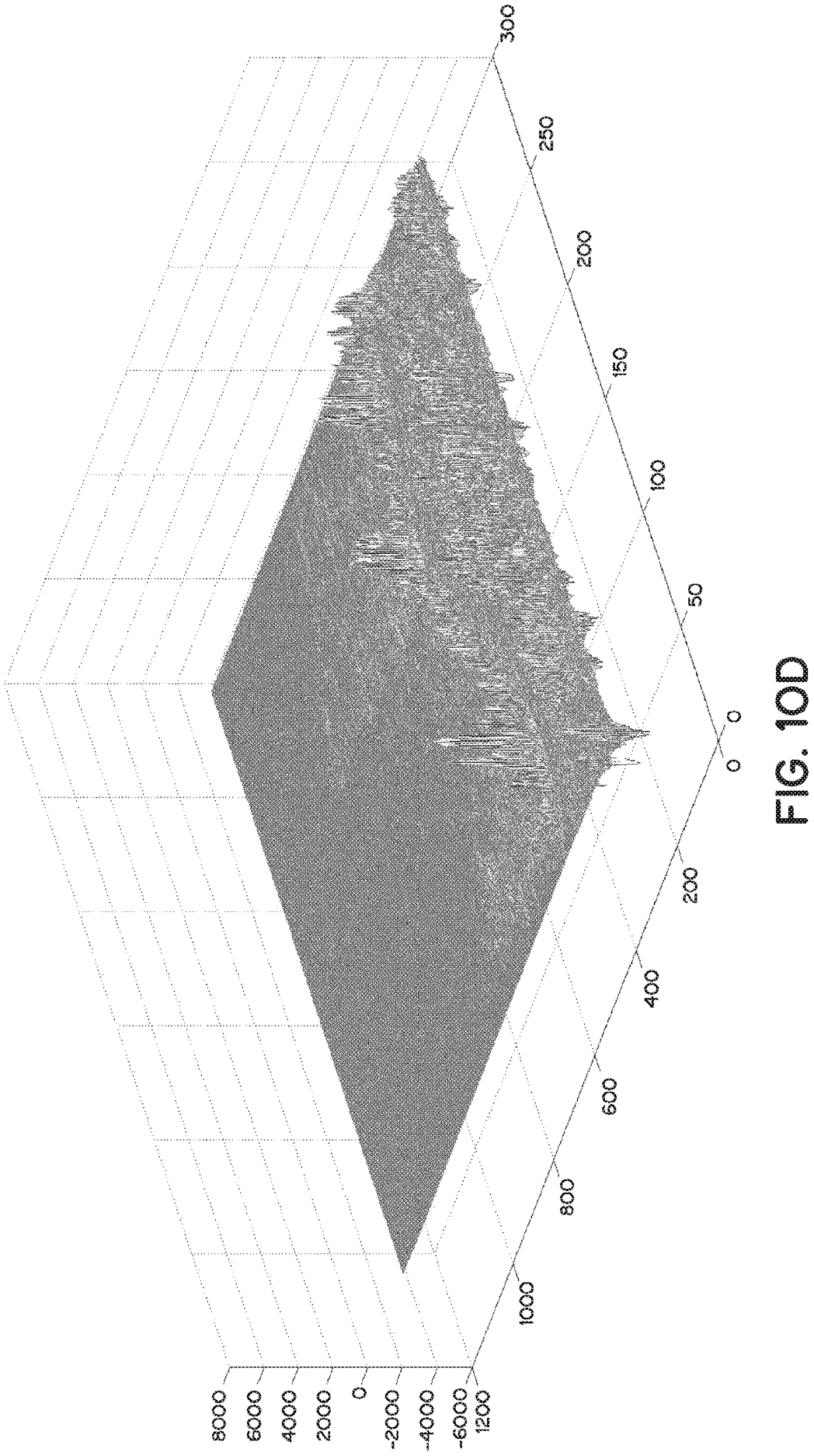
300
250
200
150
100
50
0
0
200
400
600
800
1000
1200
8000
6000
4000
2000
0
-2000
-4000
-6000

FIG. 10D

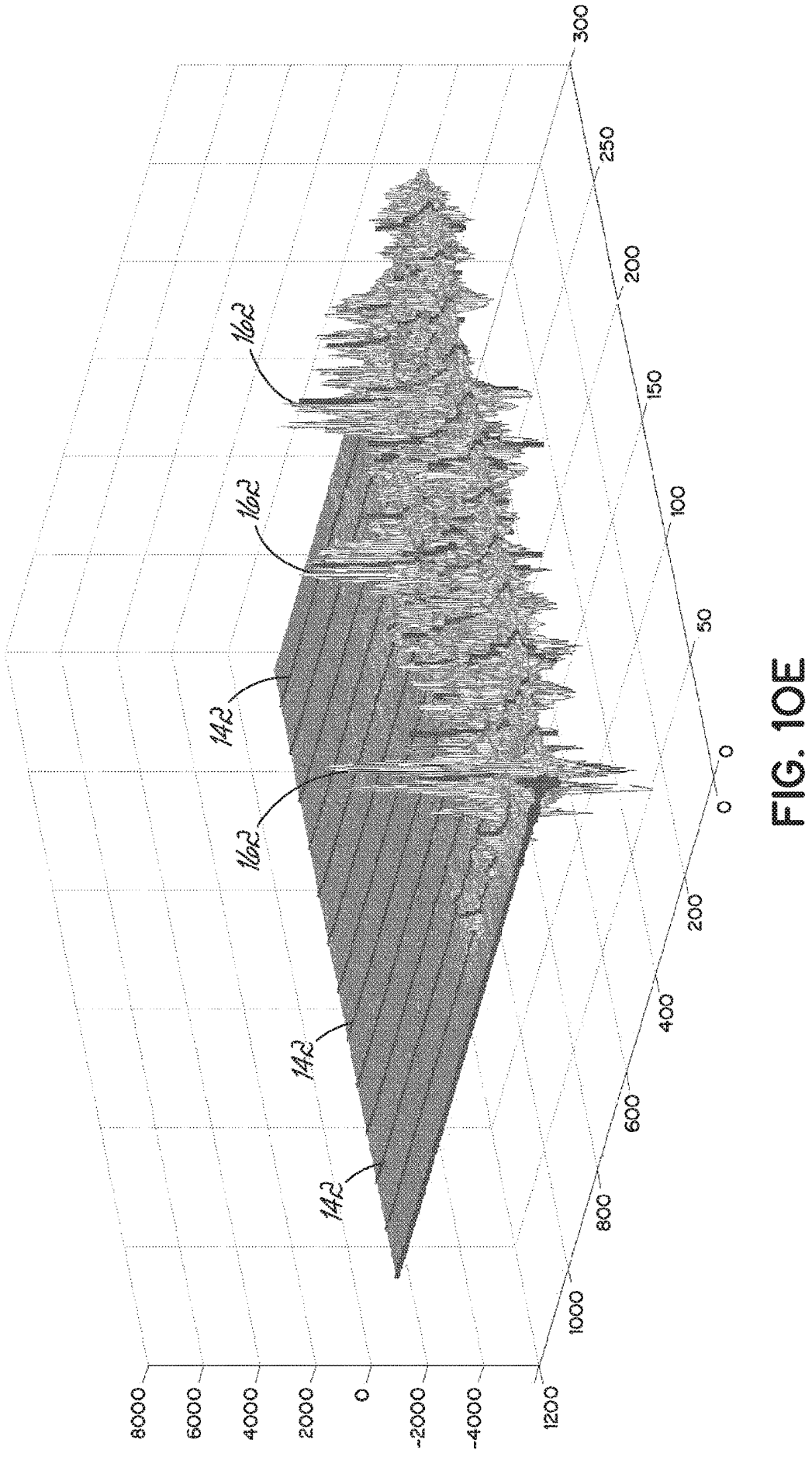
162
162
142
162
142
142
8000
6000
4000
2000
0
-2000
-4000
1200
1000
800
600
400
200
0
0
50
100
150
200
250
300

FIG. 10E

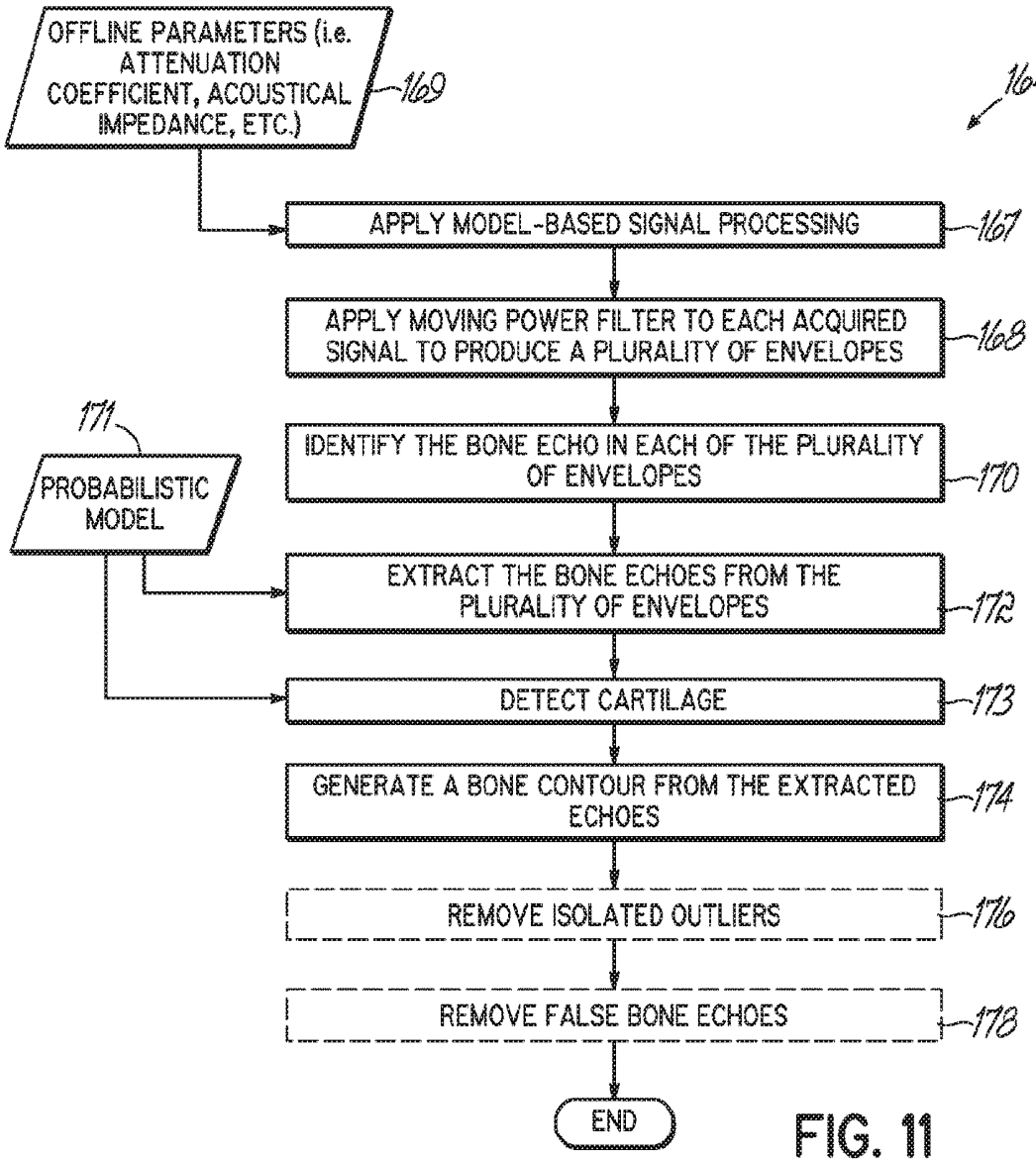
OFFLINE PARAMETERS (i.e. ATTENUATION COEFFICIENT, ACOUSTICAL IMPEDANCE, ETC.)
169
164
APPLY MODEL-BASED SIGNAL PROCESSING
167
APPLY MOVING POWER FILTER TO EACH ACQUIRED SIGNAL TO PRODUCE A PLURALITY OF ENVELOPES
168
171
PROBABILISTIC MODEL
IDENTIFY THE BONE ECHO IN EACH OF THE PLURALITY OF ENVELOPES
170
EXTRACT THE BONE ECHOES FROM THE PLURALITY OF ENVELOPES
172
DETECT CARTILAGE
173
GENERATE A BONE CONTOUR FROM THE EXTRACTED ECHOES
174
REMOVE ISOLATED OUTLIERS
176
REMOVE FALSE BONE ECHOES
178
END

FIG. 11

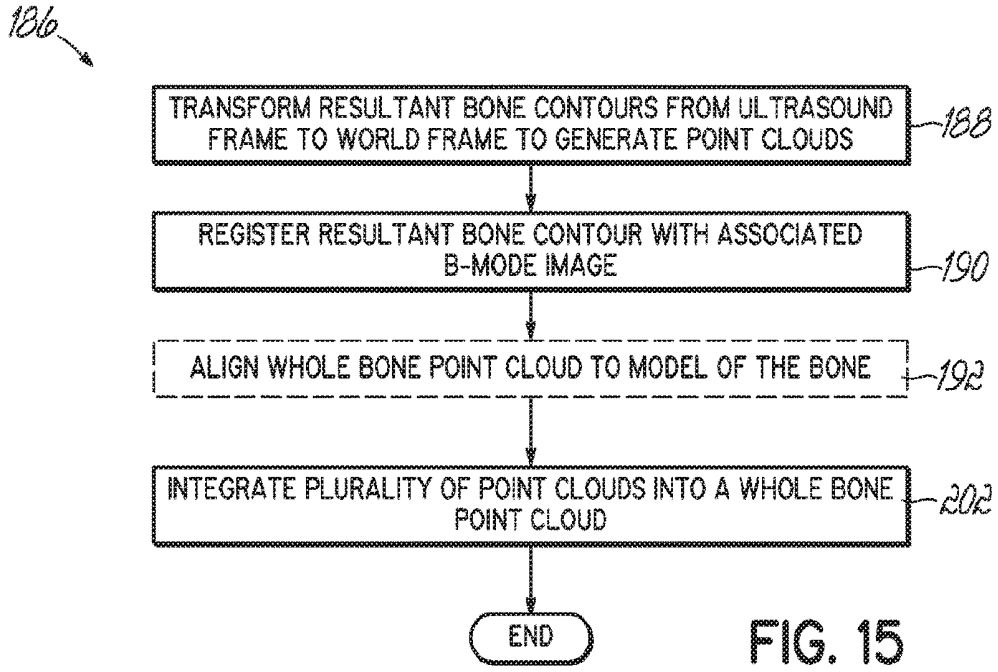
186
TRANSFORM RESULTANT BONE CONTOURS FROM ULTRASOUND FRAME TO WORLD FRAME TO GENERATE POINT CLOUDS
188
REGISTER RESULTANT BONE CONTOUR WITH ASSOCIATED B-MODE IMAGE
190
ALIGN WHOLE BONE POINT CLOUD TO MODEL OF THE BONE
192
INTEGRATE PLURALITY OF POINT CLOUDS INTO A WHOLE BONE POINT CLOUD
202
END

FIG. 15

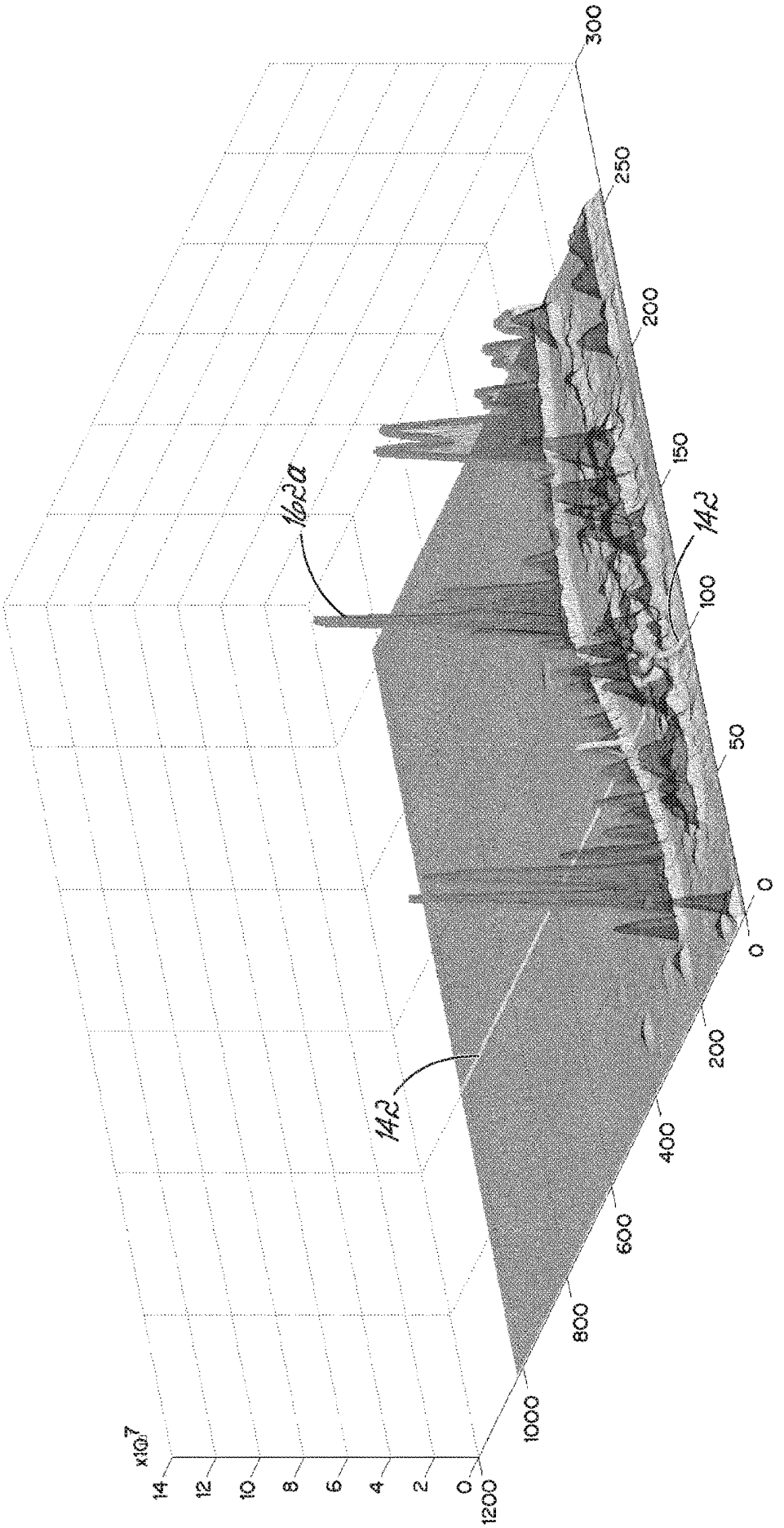
162a
142
142
x10^7
14
12
10
8
6
4
2
0
1200
1000
800
600
400
200
0
0
50
100
150
200
250
300

FIG. 12A

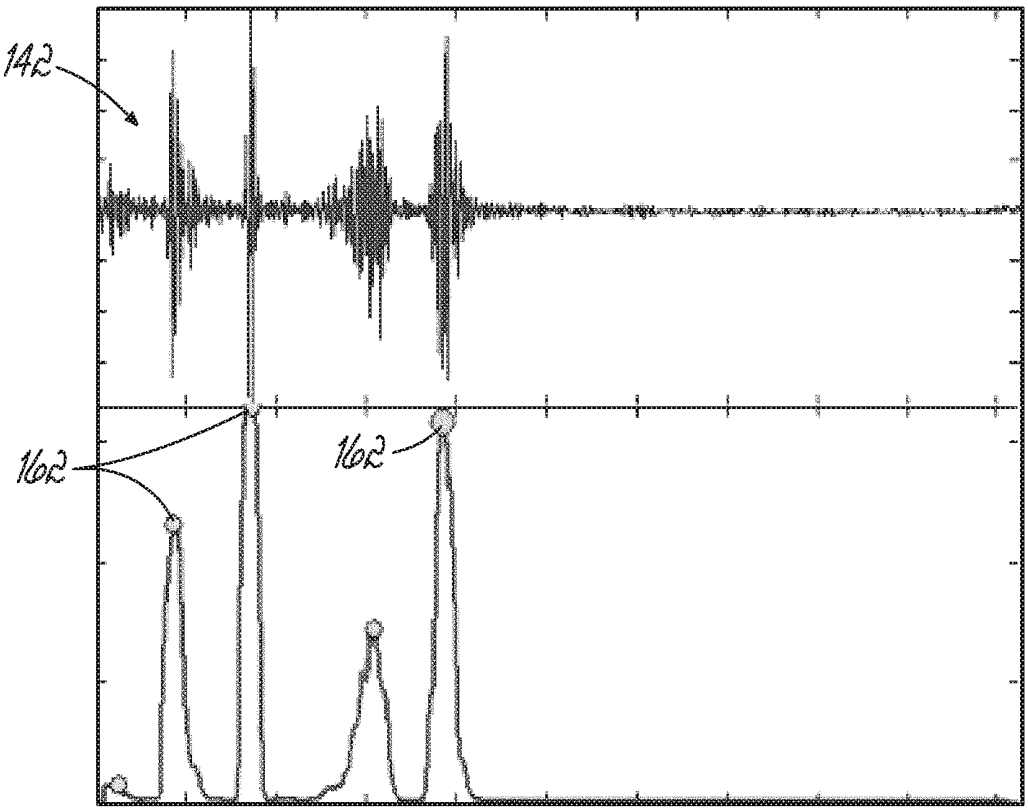

FIG. 12B

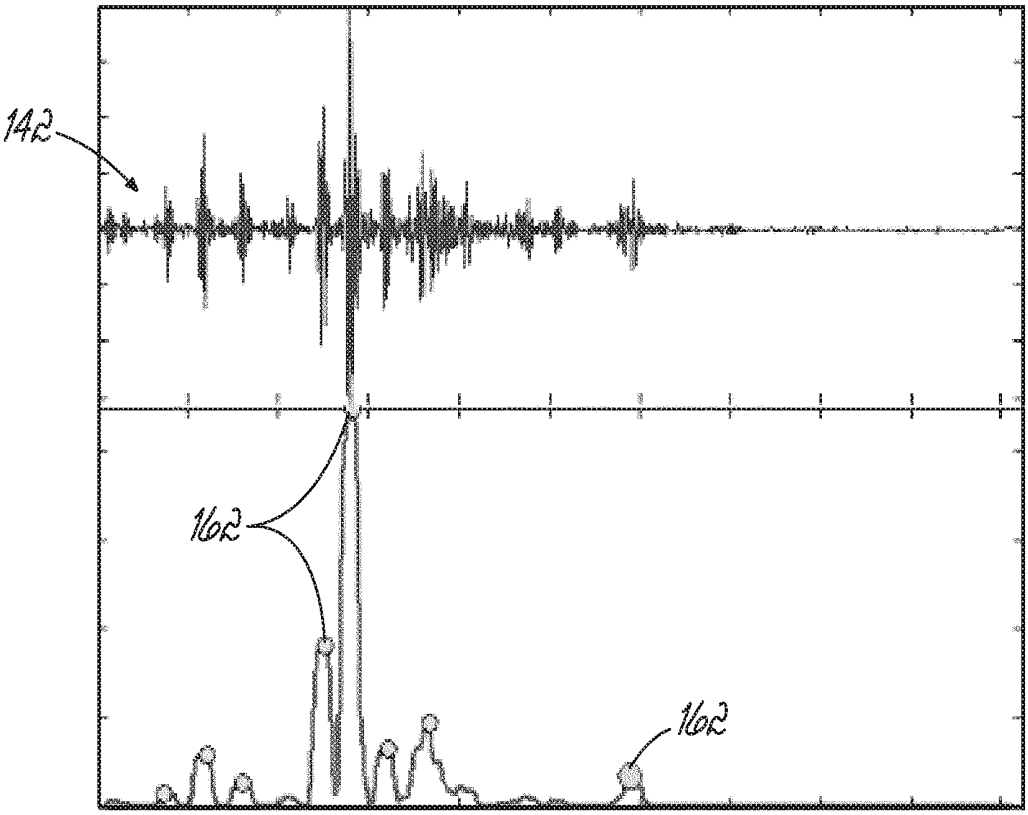

FIG. 12C

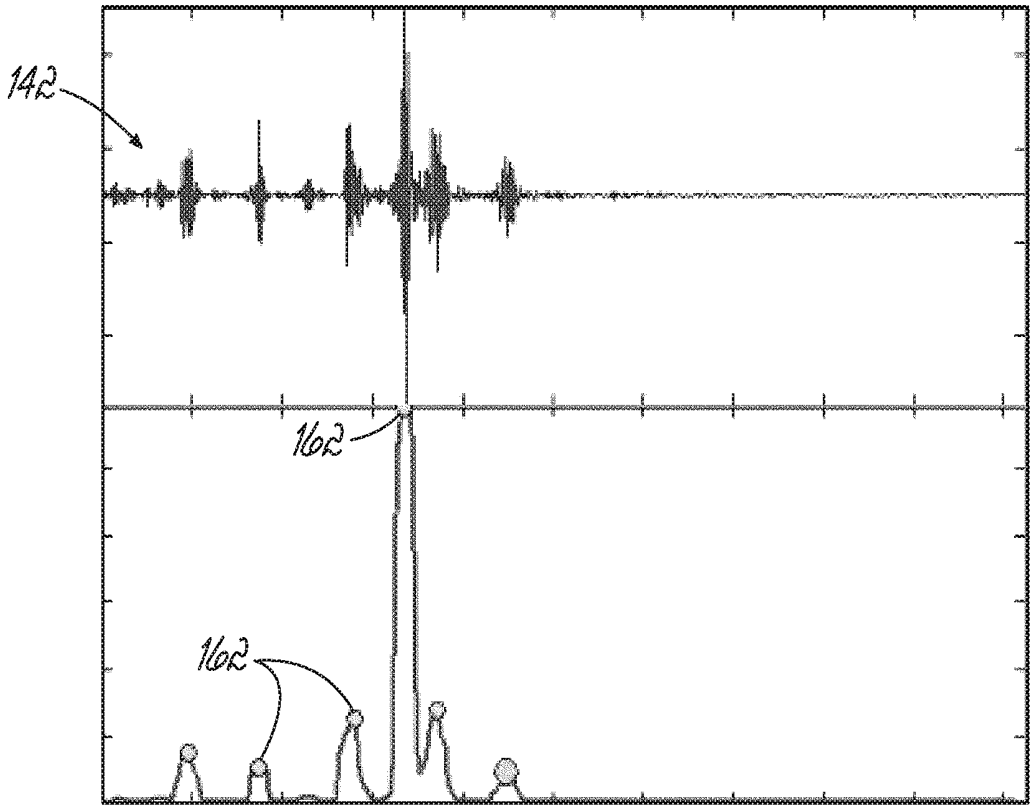

FIG. 12D

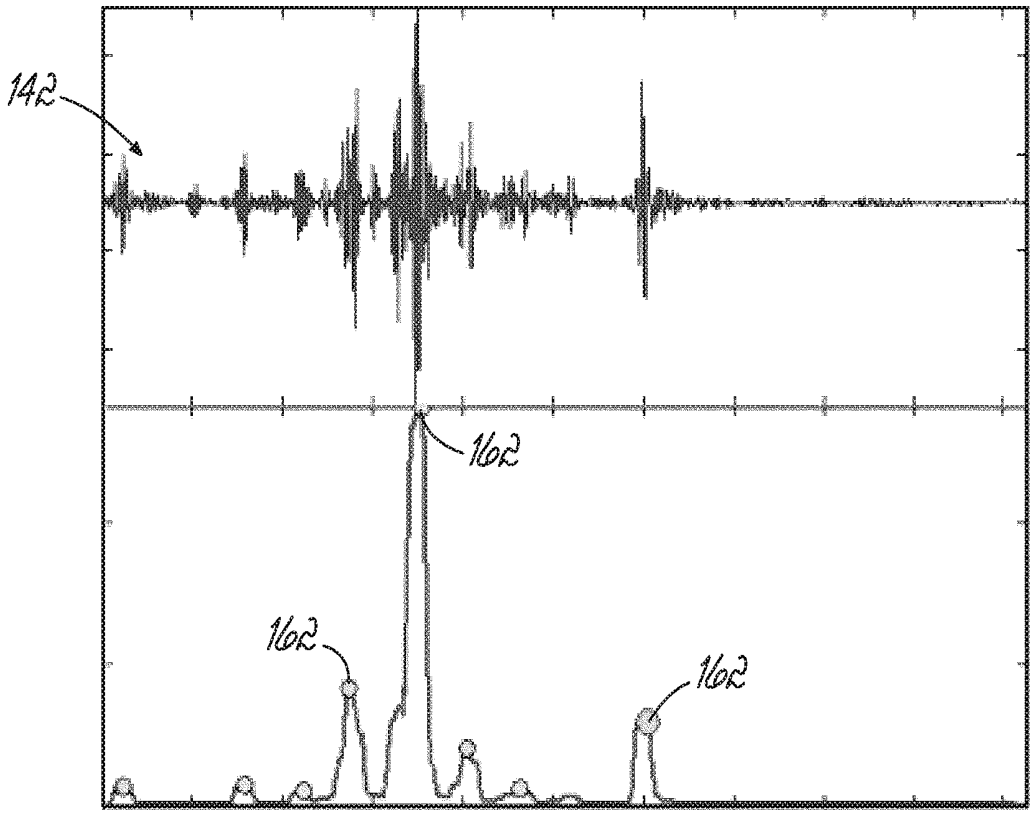

FIG. 12E

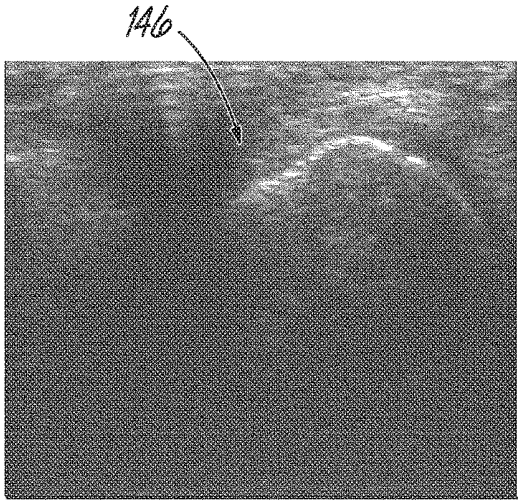

FIG. 13A

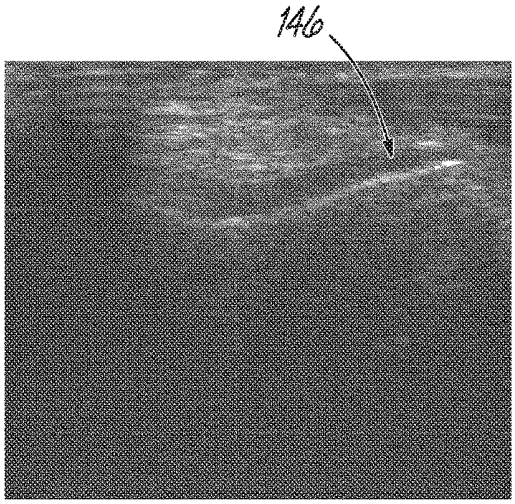

FIG. 13D

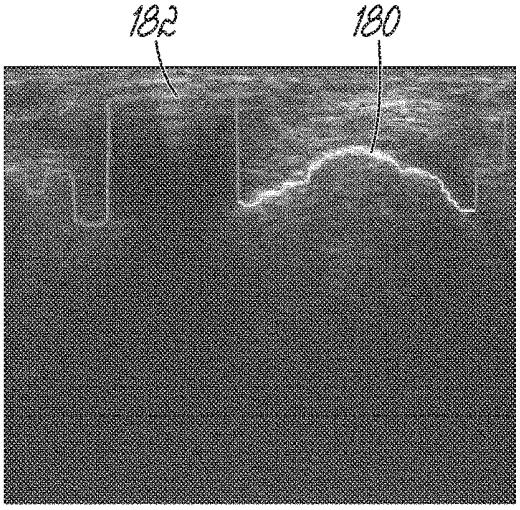

FIG. 13B

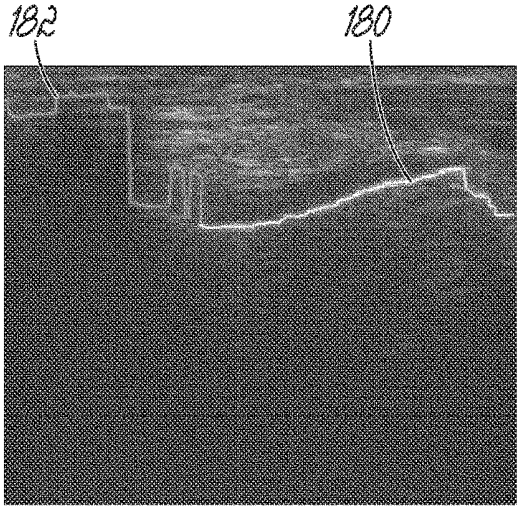

FIG. 13E

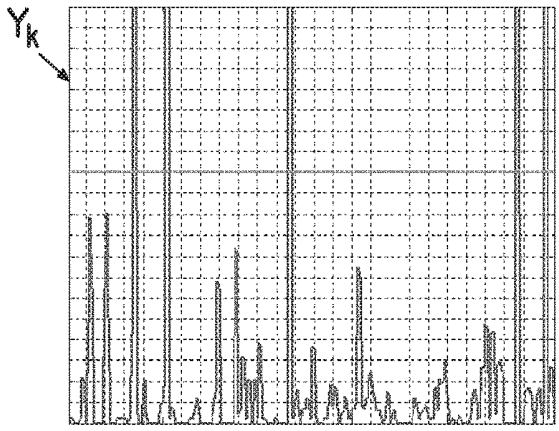

FIG. 13C

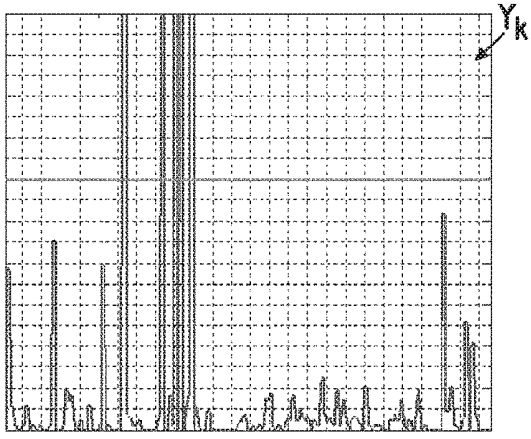

FIG. 13F

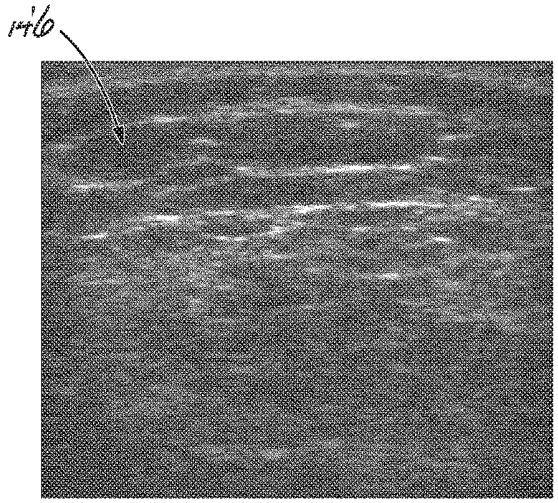

FIG. 14A

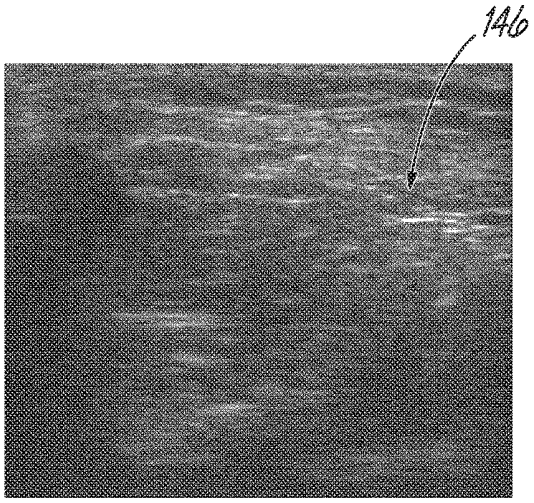

FIG. 14D

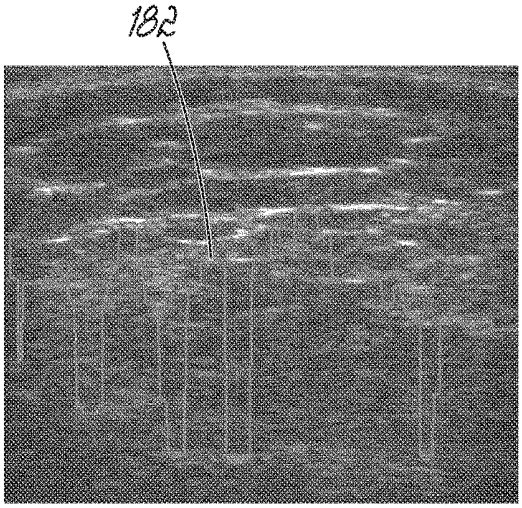

FIG. 14B

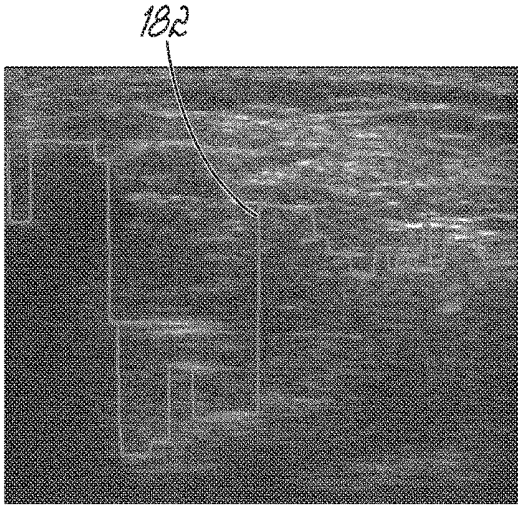

FIG. 14E

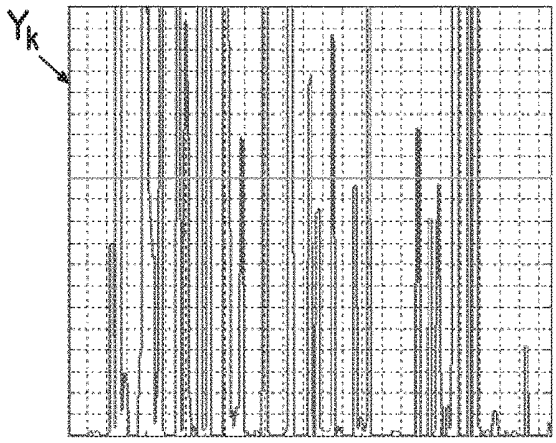

FIG. 14C

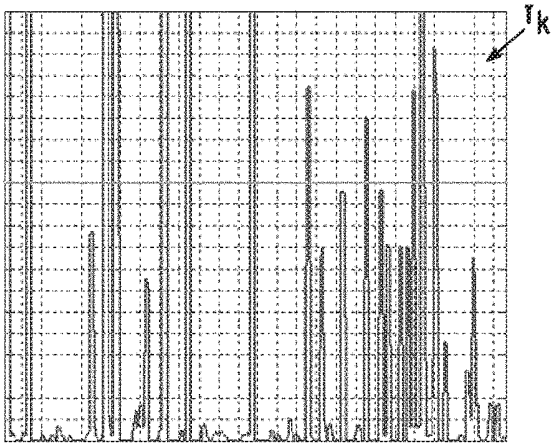

FIG. 14F

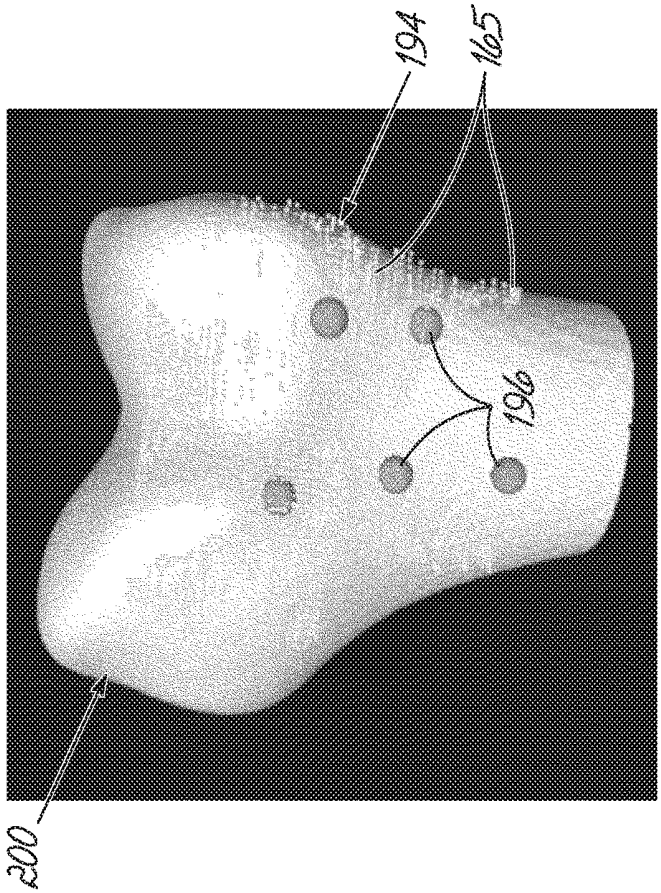

FIG. 16B

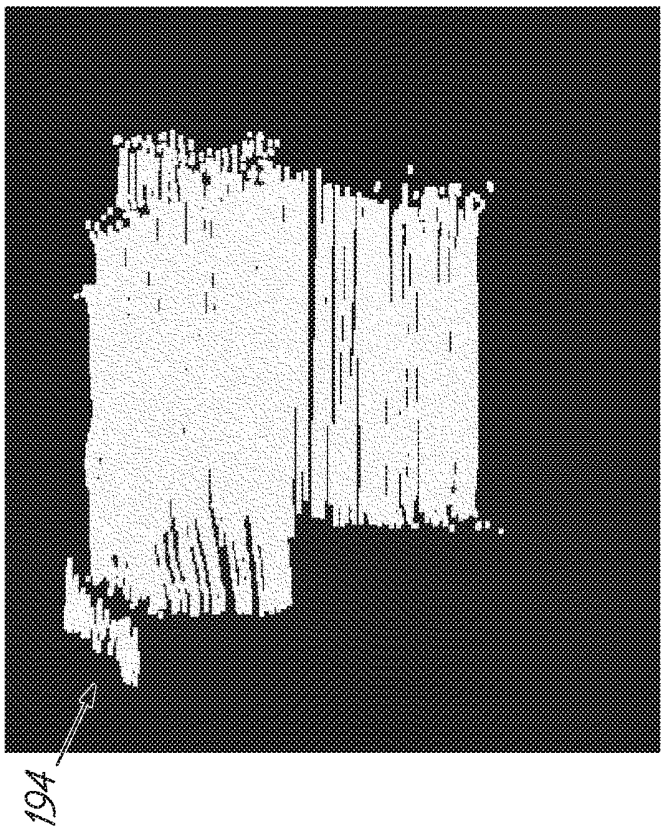

FIG. 16A

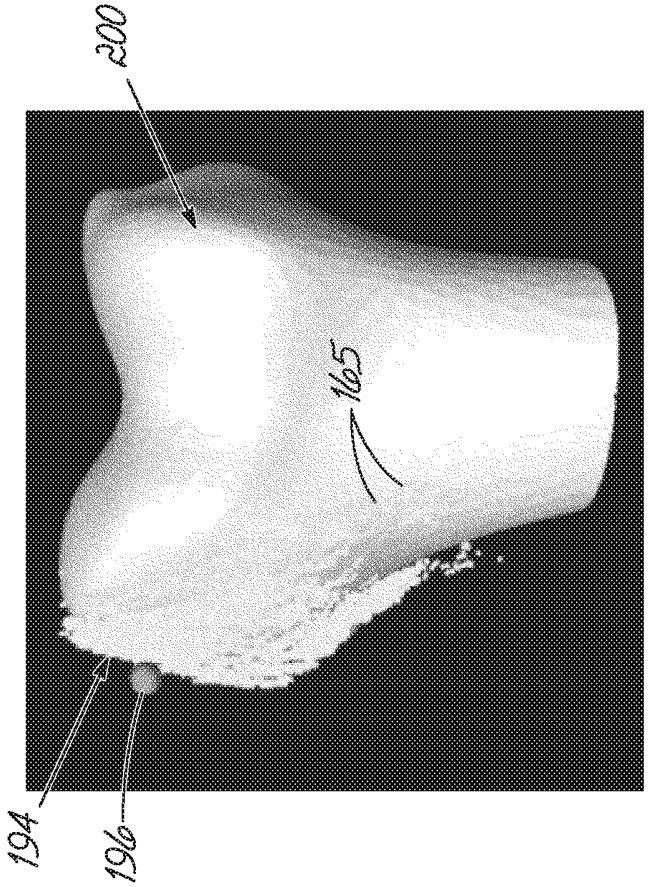

FIG. 16D

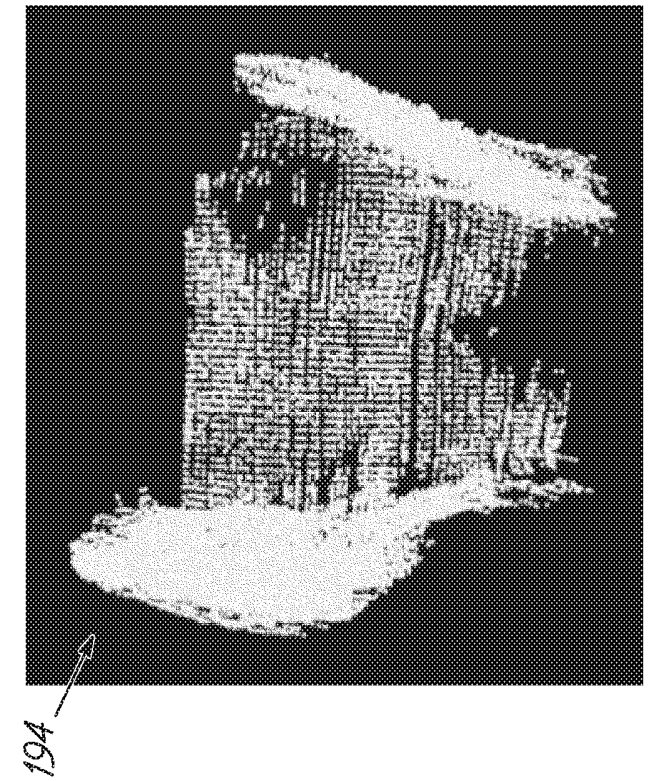

FIG. 16C

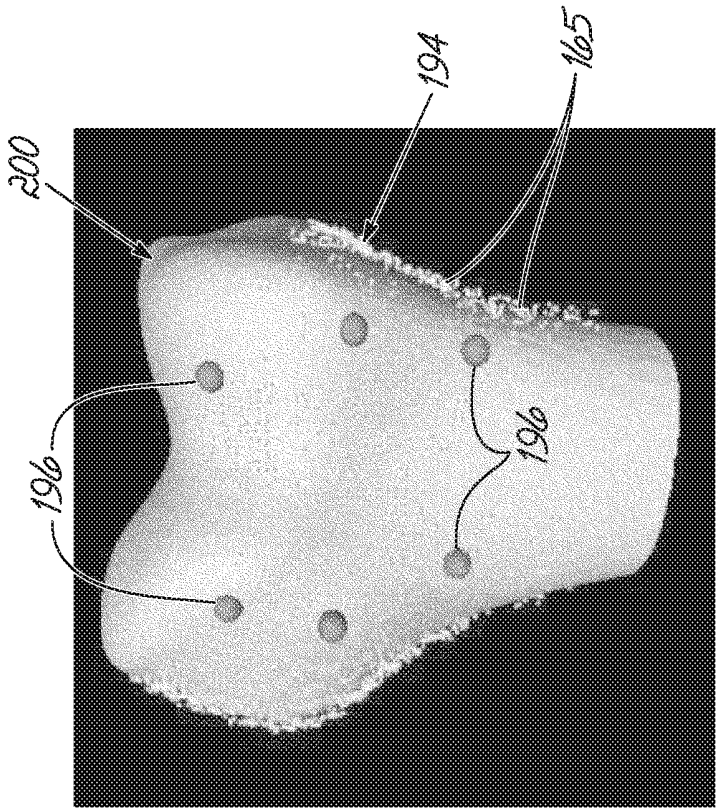

FIG. 17B

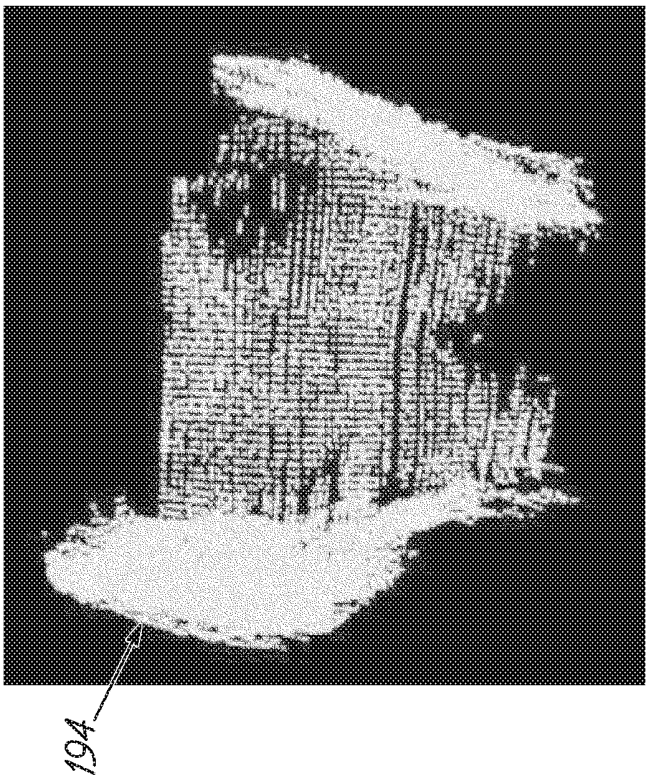

FIG. 17A

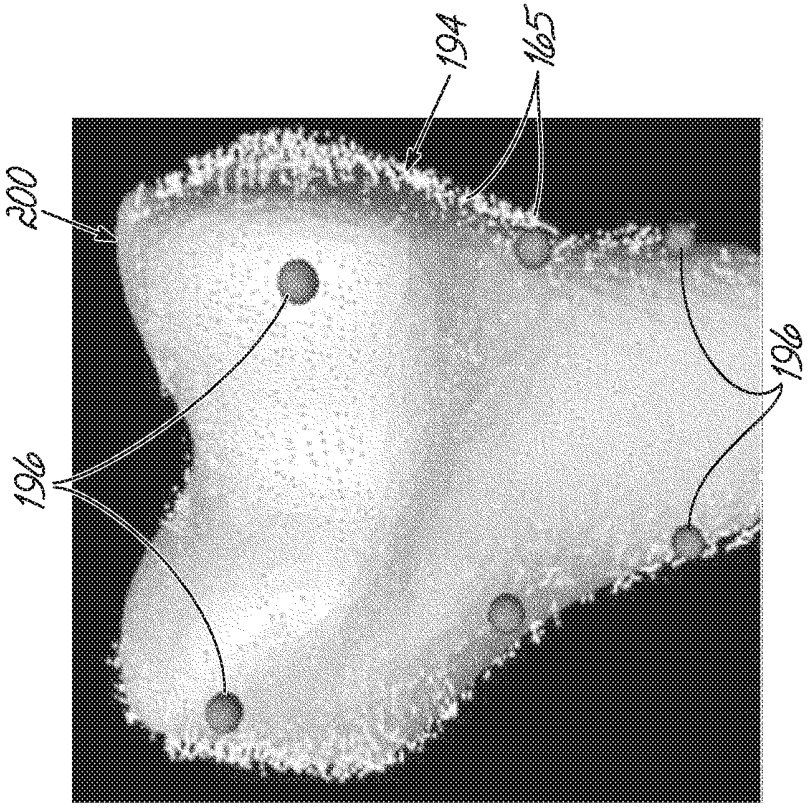

FIG. 17D

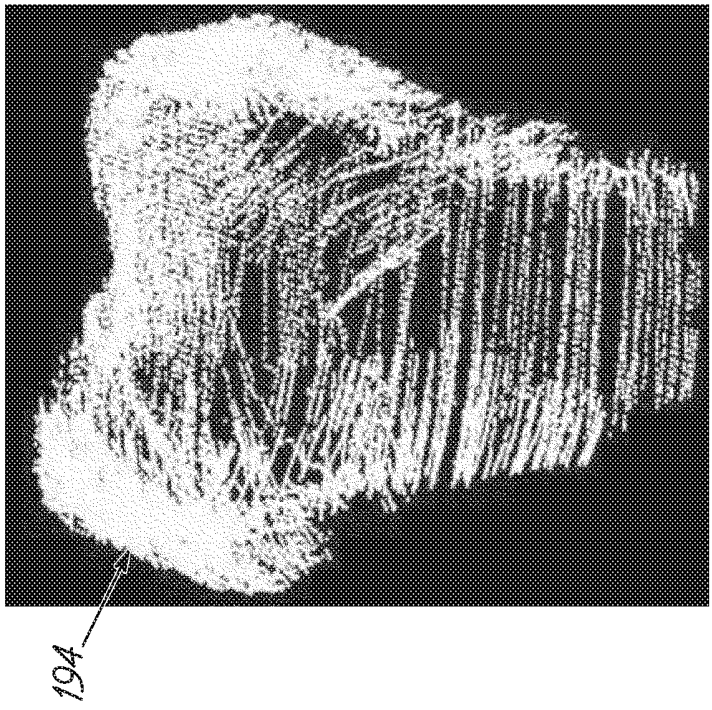

FIG. 17C

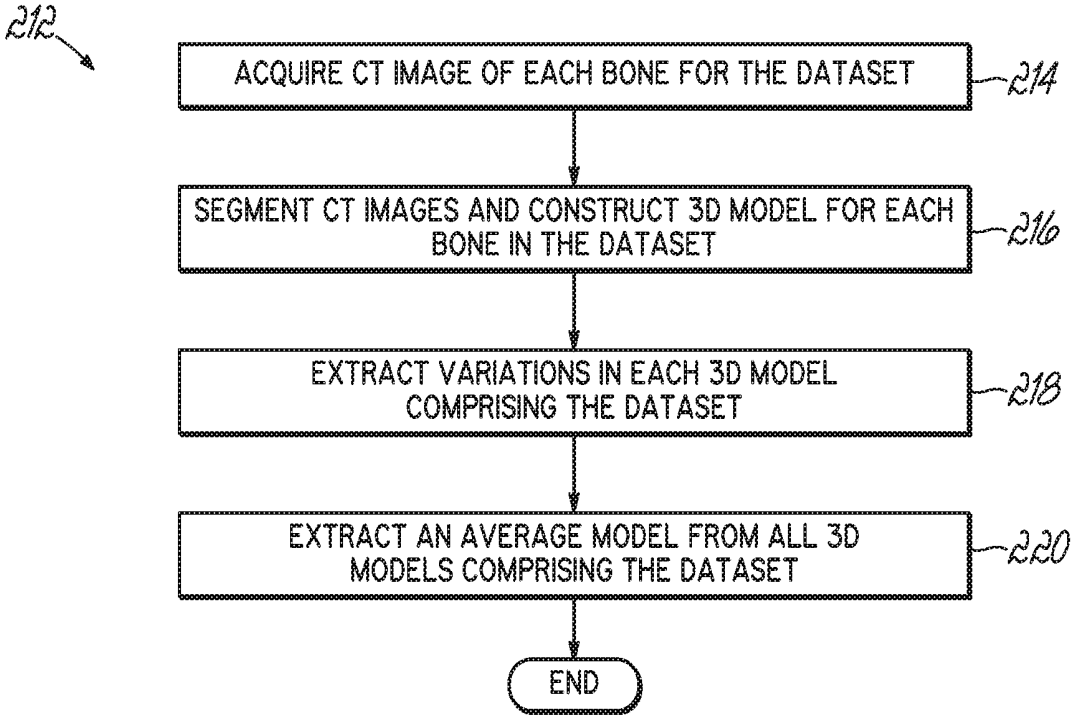
212
ACQUIRE CT IMAGE OF EACH BONE FOR THE DATASET
214
SEGMENT CT IMAGES AND CONSTRUCT 3D MODEL FOR EACH BONE IN THE DATASET
216
EXTRACT VARIATIONS IN EACH 3D MODEL COMPRISING THE DATASET
218
EXTRACT AN AVERAGE MODEL FROM ALL 3D MODELS COMPRISING THE DATASET
220
END

FIG. 18

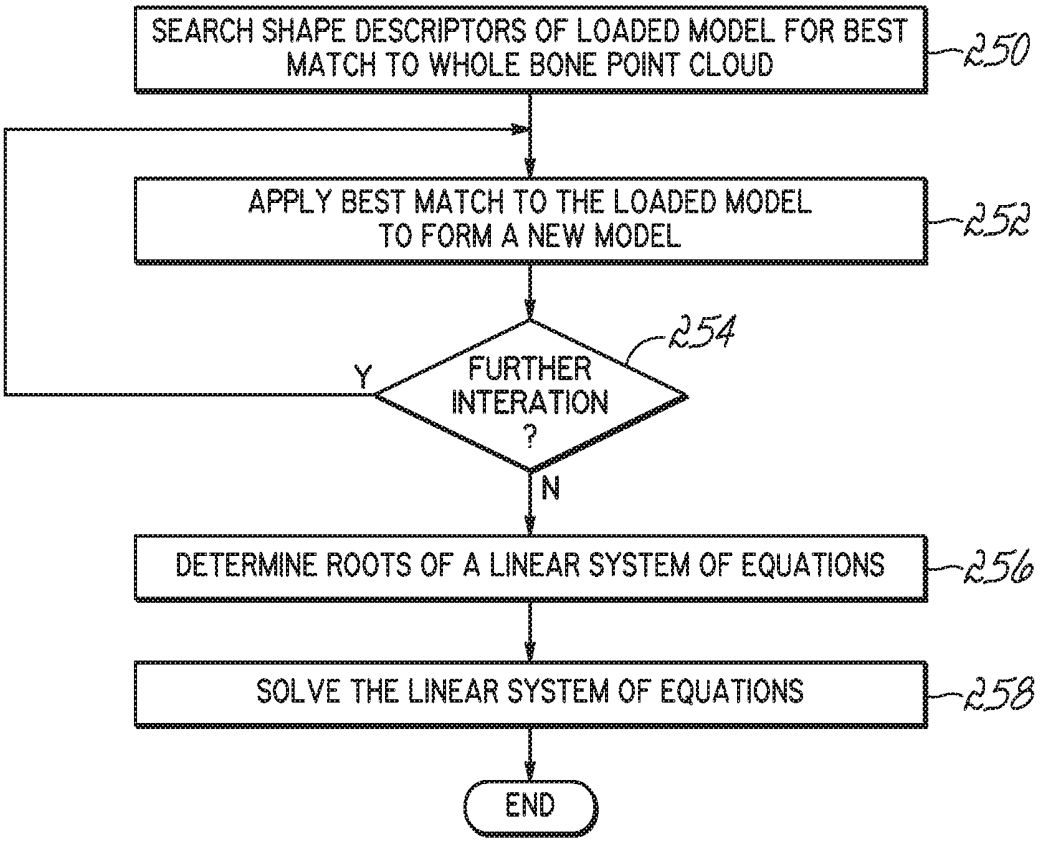
SEARCH SHAPE DESCRIPTORS OF LOADED MODEL FOR BEST MATCH TO WHOLE BONE POINT CLOUD
250
APPLY BEST MATCH TO THE LOADED MODEL TO FORM A NEW MODEL
252
254
FURTHER INTERATION ?
Y
N
DETERMINE ROOTS OF A LINEAR SYSTEM OF EQUATIONS
256
SOLVE THE LINEAR SYSTEM OF EQUATIONS
258
END

FIG. 19

METHOD AND APPARATUS FOR THREE DIMENSIONAL RECONSTRUCTION OF A JOINT USING ULTRASOUND

RELATED APPLICATIONS

[0001] This application claims priority to U.S. Provisional Patent Application No. 61/470,952 (pending), entitled "METHOD AND APPARATUS FOR THREE DIMENSIONAL RECONSTRUCTION OF JOINTS USING ULTRASOUND," filed Apr. 1, 2011, and also claims the priority of U.S. Provisional Patent Application No. 61/369,848, entitled "A NOVEL IMAGING SYSTEM FOR PATIENT-SPECIFIC 3-D KNEE MODEL RECONSTRUCTION USING ULTRASOUND," filed Aug. 2, 2010 (pending), such applications are each incorporated herein by reference in their entirety.

FIELD OF THE INVENTION

[0002] The present invention relates generally to methods of generating 3-D models of musculoskeletal systems and, more particularly, to ultrasound based 3-D bone and cartilage model reconstruction.

BACKGROUND OF THE INVENTION

[0003] The reconstruction of a 3-D model for the knee's articulating bones is a key component of computer-aided knee surgery systems. The existence of a pre-operatively acquired model enables the surgeon to pre-plan a surgery by choosing the proper implant size, calculating the femoral and tibial cutting planes, and evaluating the fit of the chosen implant. The conventional method of generating the 3-D model is segmentation of computed tomography ("CT"), or magnetic resonance imaging ("MRI") scans, which are the conventional imaging modalities for creating patient-specific 3-D bone models. The segmentation methods used are either manually, semi-automatic, or fully automated. Although these methods are produce highly accurate models, CT and MRI have inherent draw backs, i.e., both are fairly expensive procedures (especially for the MRI), and CT exposes the patient to ionizing radiation. These limitations have motivated the research of new methods for acquiring and reconstructing bone models.

[0004] One alternative method of forming patient-specific models is the use of previously acquired X-Ray images as a priori information to guide the morphing of a template bone model whose projection matches the X-Ray images. Several X-Ray based model reconstruction methodologies have been developed for the femur (including, specifically, the proximal and distal portions), the pelvis, the spine, and the rib cage.

[0005] Conventional ultrasound imaging utilizes the B-mode images. B-mode images are constructed by extracting an envelope of received scanned lines of radiofrequency ("RF") signals using the Hilbert transformation. These envelopes are then decimated (causing a drop in the resolution) and converted to grayscale (usually 256 bit) to form the final B-mode image. The conversion to grayscale results in a drop in the dynamic range of the ultrasound data.

[0006] The use of ultrasound in computer aided orthopedic surgery has gained a lot of interest in the recent decade due to its relatively low cost and radiation-free nature. More particularly, A-mode ultrasound intra-operative registration has been used for computer aided orthopedic surgery and, in limited cases, in neurosurgery. Ultrasound-MRI registration has been developed utilizing B-mode ultrasound images.

[0007] Therefore, it would be desirable to develop a method of utilizing ultrasound techniques to construct 3-D patient-specific bone and cartilage models.

SUMMARY OF THE INVENTION

[0008] The present invention overcomes the foregoing problems and other shortcomings, drawbacks, and challenges of high cost or high radiation exposure imaging modalities to generate a patient-specific model by ultrasound techniques. While the present invention will be described in connection with certain embodiments, it will be understood that the present invention is not limited to these embodiments. To the contrary, this invention includes all alternatives, modifications, and equivalents as may be included within the spirit and scope of the present invention.

[0009] In accordance with one embodiment of the present invention, a method of generating a 3-D patient-specific bone model is described. The method includes acquiring a plurality of raw radiofrequency ("RF") signals from an A-mode ultrasound scan of the bone, which is spatially tracked in 3D space. The bone contours are isolated in each of the plurality of RF signals and transformed into a point cloud. A 3-D bone model of the bone is then optimized with respect to the point cloud.

[0010] According to another embodiment of the present invention, a method for 3-D reconstruction of a bone surface includes imaging the bone with A-mode ultrasound. A plurality of RF signals is acquired while imaging. Imaging of the bone is also tracked. A bone contour is extracted from each of the plurality of RF signals. Then, using the tracked data and the extracted bone contours, a point cloud representing the surface of the bone is generated. A model of the bone is morphed to match the surface of the bone as represented by the point cloud.

[0011] In still yet another embodiment of the present invention, a computer method for simulating a surface of a bone is described. The computer method includes executing a computer program in accordance with a process. The process includes extracting a bone contour from each of a plurality of A-mode RF signals. The extracted bone contours are transformed from a local frame of reference into a point cloud in a world-frame of reference. A generalized model of the bone is compared with the point cloud and, as determined from the comparing, the generalized model is deformed to match the point cloud.

[0012] Another embodiment of the present invention is directed to a computer program product that includes a non-transitory computer readable medium and program instructions stored on the computer readable medium. The program instructions, when executed by a process, cause the computer program product to isolate a bone contour from a plurality of RF signals. The plurality of RF signals being previously acquired from a reflected A-mode ultrasound beam. The bone contours are then transformed into a point cloud and used to optimize a 3-D bone model of the bone.

[0013] Still another embodiment of the present invention is directed to a computing device having a processor and a memory. The memory includes instructions that, when executed by the processor, cause the processor to isolate a bone contour from a plurality of RF signals. The plurality of RF signals being previously acquired from a reflected

A-mode ultrasound beam. The bone contours are then transformed into a point cloud and used to optimize a 3-D bone model of the bone.

BRIEF DESCRIPTION OF THE FIGURES

[0014] The accompanying drawings, which are incorporated in and constitute a part of this specification, illustrate embodiments of the present invention and, together with the detailed description of the embodiments given below, serve to explain the principles of the present invention.

[0015] FIG. **1** is a perspective view of an ultrasound instrument in accordance with one embodiment of the present invention.

[0016] FIG. **2** is a perspective view of a hybrid probe comprising an ultrasound probe and an optical marker, in accordance with one embodiment of the present invention.

[0017] FIG. **2**A is a side elevational view of a position sensor for use with the optical marker of the hybrid probe.

[0018] FIG. **3** is a diagrammatic view of a computer system suitable for generating a 3-D patient-specific bone model from A-mode ultrasound RF signals in accordance with one embodiment of the present invention.

[0019] FIG. **4** is a flow chart illustrating one exemplary method of calibrating the optical system and generating a transformation between a local frame and a world frame.

[0020] FIGS. **5**A-**5**C are diagrammatic views of a knee joint, showing the anterior, the medial, and the posterior portions, respectively.

[0021] FIGS. **6**A-**6**F are fluoroscopic images of the knee joint in a plurality of degrees of flexion.

[0022] FIG. **7** is a flow chart illustrating one exemplary method of acquiring A-mode ultrasound RF signal and generating the 3-D patient-specific bone model.

[0023] FIG. **8** is a diagrammatic view of the method of acquiring A-mode ultrasound RF signals in accordance with FIG. **7**.

[0024] FIG. **9** is a B-mode ultrasound image of a knee joint, which may optionally be shown from the A-mode ultrasound RF signal.

[0025] FIG. **10**A is an example of a raw RF signal as acquired by one transducer of the transducer array of an ultrasound probe.

[0026] FIG. **10**B is the ultrasound frame illustrates select ones of the RF signals overlaid the B-mode ultrasound image of FIG. **9**.

[0027] FIG. **100** is the ultrasound frame of FIG. **9**B with a bone echo contour identified.

[0028] FIG. **10**D is a 3-D rendering of the RF signals acquired in a data frame, which is shown in the B-mode image format in FIG. **100**.

[0029] FIG. **10**E is another 3-D rendering of an ultrasound frame with select ones of the RF signals delineated.

[0030] FIG. **11** is a flow chart illustrating one exemplary method of identifying and extracting the bone echo from the A-mode ultrasound RF signal.

[0031] FIG. **12**A is a 3-D rendering of an ultrasound frame after envelope detection.

[0032] FIGS. **12**B-**12**E respectively illustrate four exemplary envelopes of the sampled A-mode ultrasound RF signal, with the echoes identified in each envelope.

[0033] FIGS. **13**A and **13**D are B-mode ultrasound frames calculated from exemplary A-mode ultrasound RF signals.

[0034] FIGS. **13**B and **13**E are ultrasound frames corresponding to FIGS. **13**A and **13**-D, respectively, with a bone contour identified before noise removal and overlain on the B-mode image.

[0035] FIGS. **13**C and **13**F are plots of the local standard deviation of the bone contours of FIGS. **13**B and **13**E, respectively.

[0036] FIGS. **14**A and **14**D are ultrasound frames illustrating exemplary B-mode images constructed from A-mode ultrasound RF signals, and in which no bone tissue was scanned.

[0037] FIGS. **14**B and **14**E are ultrasound frames corresponding to FIGS. **14**A and **14**D, respectively, with the noisy false bone contours shown.

[0038] FIGS. **14**C and **14**F are plots of the local standard deviation of the last echoes of FIGS. **14**B and **14**E, respectively.

[0039] FIG. **15** is a flow chart illustrating one exemplary method of generating a bone point cloud from the isolated bone contours.

[0040] FIGS. **16**A, **16**C, **17**A, and **17**C are exemplary bone point clouds, generated in accordance with one embodiment of the present invention.

[0041] FIGS. **16**B, **16**D, **17**B, and **17**D are examples in which the bone point clouds of FIGS. **16**A, **16**C, **17**A, and **17**C, respectively, are aligned to a bone model.

[0042] FIG. **18** is a flow chart illustrating one exemplary method of generating a statistical atlas of bone models.

[0043] FIG. **19** is a flow chart illustrating one exemplary method of optimizing a bone model to the bone point cloud.

DETAILED DESCRIPTION OF THE EMBODIMENTS OF THE INVENTION

[0044] The various embodiments of the present invention are directed to methods of generating a 3-D patient-specific bone model. To generate the 3-D patient-specific model, a plurality of raw RF signals is acquired using A-mode ultrasound acquisition methodologies. A bone contour is then isolated in each of the plurality of RF signals and transformed into a point cloud. The point clouds may then be used to optimize a 3-D bone model of the bone such that the patient-specific model may be generated.

[0045] Turning now to the figures, and in particular to FIG. **1**, one embodiment of an ultrasound instrument **50** for use with one or more embodiments of the present invention is shown. The ultrasound instrument **50** should be configurable such that the user may access acquired RF ultrasound data. One suitable instrument may, for example, include the diagnostic ultrasound model SonixRP by Ultrasonix Inc. (Richmond, British Columbia, Canada). The ultrasound instrument **50** includes a housing **52** containing a controller, (for example, a computer **54**), an energy or power source (not shown), a user input device **56**, an output device (for example, a monitor **58**), and at least one ultrasound probe **60**. The housing **52** may include caster wheels **62** for transporting the ultrasound instrument **50** within the medical facility.

[0046] The at least one ultrasound probe **60** is configured to acquire ultrasound raw radiofrequency ("RF") signals, and is shown in greater detail in FIG. **2**. The ultrasound probe **60**, such as the particular embodiment shown, may be a high resolution linear transducer with a center frequency of 7.5 MHz, as is conventionally used in musculoskeletal procedures. The sampling frequency used in digitizing ultra-

sound echo may be, for example, 20 MHz and must be at least twice the maximum ultrasound frequency. Generally, the ultrasound probe **60** includes a body **64** that is coupled to the ultrasound instrument housing **52** (FIG. **1**) by a cable **66**. The body **64** further includes a transducer array **68** configured to transmit an ultrasound pulse and to receive reflected ultrasound RF energy. The received RF echo is transmitted along the cable **66**, to the computer **54** of the ultrasound instrument **50** (FIG. **1**) for processing in accordance with an embodiment of the present invention.

[0047] The computer **54** of the ultrasound instrument **50** (FIG. **1**), as shown in FIG. **3**, may be considered to represent any type of computer, computer system, computing system, server, disk array, or programmable device such as multi-user computers, single-user computers, handheld devices, networked devices, or embedded devices, etc. The computer **54** may be implemented with one or more networked computers **70** or networked storage devices **72** using one or more networks **74**, e.g., in a cluster or other distributed computing system through a network interface **76** (illustrated as "NETWORK I/F"). For brevity's sake, the computer **54** will be referred to simply as "computer," although it should be appreciated that the term "computing system" may also include other suitable programmable electronic devices consistent with embodiments of the present invention.

[0048] The computer **54** typically includes at least one processing unit **78** (illustrated as "CPU") coupled to a memory **80** along with several different types of peripheral devices, e.g., a mass storage device **82**, the user interface **84** (illustrated as "User I/F," which may include the input device **56** (FIG. **1**) and the monitor **58** (FIG. **1**)), and the Network I/F **76**. The memory **80** may include dynamic random access memory ("DRAM"), static random access memory ("SRAM"), non-volatile random access memory ("NVRAM"), persistent memory, flash memory, at least one hard disk drive, and/or another digital storage medium. The mass storage device **82** is typically at least one hard disk drive and may be located externally to the computer **54**, such as in a separate enclosure or in one or more of the networked computers **70**, one or more of the networked storage devices **72** (for example, a server)

[0049] The CPU **78** may be, in various embodiments, a single-thread, multi-threaded, multi-core, and/or multi-element processing unit (not shown) as is well known in the art. In alternative embodiments, the computer **54** may include a plurality of processing units that may include single-thread processing units, multi-threaded processing units, multi-core processing units, multi-element processing units, and/or combinations thereof as is well known in the art. Similarly, the memory **80** may include one or more levels of data, instruction, and/or combination caches, with caches serving the individual processing unit or multiple processing units (not shown) as is well known in the art.

[0050] The memory **80** of the computer **54** may include an operating system **81** (illustrated as "OS") to control the primary operation of the computer **54** in a manner that is well known in the art. The memory **80** may also include at least one application, component, algorithm, program, object, module, or sequence of instructions, or even a subset thereof, will be referred to herein as "computer program code" or simply "program code," (illustrated as same, **83**). Program code **83** typically comprises one or more instructions that are resident at various times in the memory **80** and/or the mass storage device **82** of the computer **54**, and that, when read and executed by the CPU **78**, causes the computer **54** to perform the steps necessary to execute steps or elements embodying the various aspects of the present invention.

[0051] Those skilled in the art will recognize that the environment illustrated in FIG. **3** is not intended to limit the present invention. Indeed, those skilled in the art will recognize that other alternative hardware and/or software environments may be used without departing from the scope of the present invention.

[0052] Returning again to FIG. **2**, the ultrasound probe **60** has mounted thereto a tracking marker **86**, which, for purposes of illustration only, is shown as an optical marker, configured to spatially register the motion of the ultrasound probe **60** during signal acquisition. The tracking marker **86** may be comprised of a plurality of reflective portions **90**, which are described in greater detail below. The tracked probe constitutes a hybrid probe **94**. In other embodiments, the tracking marker and associated system may be electromagnetic, RF, or any other known 3-D tracking system.

[0053] The optical marker **86** is operably coupled to a position sensor **88**, one embodiment of which is shown in FIG. **2**A. In use, the position sensor **88** emits energy (for example, infrared light) in a direction toward the optical marker **86**. Reflective portions **90** of the optical marker **86** reflect the energy back to the position sensor **88**, which then triangulates the 3-D position and orientation of the optical marker **86**. One example of a suitable optical tracking system is the Polaris model manufactured by Northern Digital Inc. (Waterloo, Ontario, Canada).

[0054] The optical marker **86** is rigidly attached to the ultrasound probe **60** and is provided a local coordinate frame of reference ("local frame" **92**). Additionally, the ultrasound probe **60** is provided another local coordinate frame of reference ("ultrasound frame"). For the sake of convenience, the combination optical marker **86** with the ultrasound probe **60** is referred to as the "hybrid probe" **94**. The position sensor **88**, positioned away from the hybrid probe **94**, determines a fixed world coordinate frame ("world frame").

[0055] Operation of the optical tracking system (the optical marker **86** with the position sensor **88**) with the ultrasound probe **60**, once calibrated, is configured to determine a transformation between the local and ultrasound coordinate frames.

[0056] Turning now to FIG. **4**, with reference also to FIG. **2**, a method **100** of calibrating the optical tracking system according to one embodiment of the present invention is described. To calibrate the optical marker **86** with the position sensor **88**, for real-time tracking of the hybrid probe **94**, a homogeneous transformation T_{OP}^{W} between the local frame, OP, and the world frame, W, is needed. The calibration method **100** begins with determining a plurality of calibration parameters (Block **102**). In the particular illustrative example, four parameters are used and include: $P_{trans\text{-}origin}$, i.e., a point of origin on the transducers array **68**; L_{trans}, i.e., a length of the transducer array **68**; $\hat{u}_x$, i.e., a unit vector along the length of the transducer array **68**; **4**) $\hat{u}_y$, i.e., a unit vector in a direction that is perpendicular to the length of the transducer array **68**. These calibration points and vectors are relative to the local frame **92** ("OP").

[0057] The hybrid probe is held in a fixed position while the position sensor **88** optical camera acquires a number of position points, including, for example: P_{trans1}, i.e., a first

end of the transducer array **68**; P_{trans2}, i.e., a second end of the transducer array **68**; and P_{plane}, i.e., a point on the transducer array **68** that is not collinear with P_{trans1} and P_{trans2} (Block **104**). The homogeneous transformation between OP and W, T_{OP}^{W}, is the recorded (Block **106**). The plurality of calibration parameters are then calculated (Block **108**) from the measured number of points and the transformation, T_{OP}^{W}, as follows:

$$T_W^{OP} = (T_{OP}^W)^{-1} \quad (1)$$

$$P_{trans-origin} = T_W^{OP} P_{trans1} \quad (2)$$

$$L_{trans} = \|P_{trans2} - P_{trans1}\| \quad (3)$$

$$\hat{u}_x = T_W^{OP} \frac{P_{trans2} - P_{trans1}}{\|P_{trans2} - P_{trans1}\|} \quad (4)$$

$$\hat{u}_y = \frac{(P_{plane} - P_{trans1}) \times (P_{trans2} - P_{trans1})}{\|(P_{plane} - P_{trans1}) \times (P_{trans2} - P_{trans1})\|} \quad (5)$$

[0058] With the plurality of calibration parameters determined, the hybrid probe **94** may be used to scan a portion of a patient's musculoskeletal system while the position sensor **88** tracks the physical movement of the hybrid probe **94**.

[0059] Because of the high reflectivity and attenuation of bone to ultrasound, ultrasound energy does not penetrate bone tissues. Therefore, soft tissues lying behind bone cannot be imaged and poses a challenge to ultrasound imaging of a joint. For example, as shown in FIGS. **5**A-**5**C, the knee joint **114** is formed of three articulating bones: the femur **116**, the tibia **118**, and the patella **120**, with the fibula **122** shown as environment. These bones **116**, **118**, **120** articulate together in two sub-joints: (1) the tibio-femoral joint **136** is formed by the articulation of the femur **116** with the tibia **118** at the respective condyles **124**, **126**, **128**, **130** and (2) the patello-femoral joint **138** is formed by the articulation of the patella **120** with the femur **116** at the patellar surface **132** of the femur **116** and the articular surface **134** of the patella **120**. During flexion-extension motions of the knee joint **114**, portions of one or more articulating surfaces of the bones **116**, **118**, **120** are visible to the ultrasound beam, while other articulating surfaces are occluded. FIGS. **6**A-**6**F include various fluoroscopic images of one patient's knee joint **114**, showing the articulating surfaces at a plurality of degrees of flexion.

[0060] To acquire ultrasound images of a majority of the articulating surfaces, at least two degrees of flexion are required, including, for example, a full extension (FIG. **6**A) and a deep knee bend (FIG. **6**F) (or 90° flexion (FIG. **6**E) if a deep knee bend is too difficult for the patient to achieve). That is, when the knee joint **114** is in the full extension (FIG. **6**A), the posterior portions of the distal femur **116** and the proximal tibia **118** are accessible to the ultrasound beam. When the knee joint **114** is in the deep knee bend (FIG. **6**F), the anterior surface of the distal femur **116**, the trochlear grove **140**, most of the inferior surface of the femoral condyles **124**, **126**, the anterior superior surface of the tibia **118**, and the anterior surface of the tibia **118** are accessible to the ultrasound beam. Both the medial and lateral parts of the femur **116** and tibia **118** are visible at all flexion angles of the knee joint **114**.

[0061] Turning now to FIG. **7**, one method **150** of acquiring data for construction of a 3-D patient-specific bone model is described. The method begins with acquiring a plurality of RF signals from an A-mode ultrasound beam scan of a bone. To acquire the RF signals for creating the 3-D patient-specific model of the knee joint **114**, the patient's knee joint **114** is positioned and held in one of the two or more degrees of flexion (Block **152**). The hybrid probe **94** is positioned, at two or more locations, on the patient's epidermis **144** adjacent to the knee joint **114** for acquisition of the A-mode RF signal **142**, one example, as shown in FIG. **8**. Although the acquired signal includes a plurality of RF signals, for convenience, the RF signals are sometimes referred to herein in singular form.

[0062] As shown in FIG. **8**, with reference also to FIG. **7**, the position of the patient's knee joint **114** is held stationary to avoid motion artifacts during image acquisition. Should motion occur, scans may be automatically aligned to the statistically-most likely position given the data acquired. Furthermore, holding the knee stationary and compensating for movement removes the need for invasive fiducial bone markers or high-error skin markers. In some embodiments, B-mode images, similar to the one shown in FIG. **9**, may also be processed from the gathered data (Block **154**) for subsequent visualization and overlain with the bone contours, as described in detail below.

[0063] When the RF signal **142**, and if desired B-mode image, acquisition is complete for the first degree of flexion, the patient's knee **114** is moved to another degree of flexion and the reflected RF signal **142** acquired (Block **156**). Again, if desired, the B-mode image may also be acquired (Block **158**). The user then determines whether acquisition is complete or whether additional data is required (Block **160**). That is, if visualization of a desired surface of one or more bones **116**, **118**, **120** is occluded ("NO" branch of decision block **160**), then the method returns to acquire additional data at another degree of flexion (Block **156**). If the desired bone surfaces are sufficiently visible ("YES" branch of decision block **160**), then the method **150** continues.

[0064] FIG. **8** illustrates acquisition of the RF signal **142** in yet another manner. That is, while the patient's leg is in full extension (shown in phantom), the hybrid probe **94** is positioned at two or more locations on the patient's epidermis **144** adjacent to the knee joint **114**. The patient's leg is then moved to a second degree of flexion (90° flexion is shown in solid) and the hybrid probe **94** again positioned at two or more locations on the patient's epidermis **144**. All the while, the position sensor **88** tracks the location of the hybrid probe **94** in the 3-D space. Resultant RF signal profiles, bone models, bone contours, and so forth may be displayed on the monitor **58** during and the monitor **58'** after the model reconstruction.

[0065] After all data and RF signal acquisition is complete, the computer **54** (FIG. **3**) is operated to automatically isolate that portion of the RF signal, i.e., the bone contour, from each of the plurality of RF signals. In that regard, the computer **54** (FIG. **3**) may sample the echoes comprising the RF signals to extract a bone contour for generating a 3-D point cloud **165** (FIG. **16**B) (Block **164**). More specifically, and with reference now to FIGS. **10**A-**10**E and **11**, with continued reference to FIGS. **7**-**9**, one method **164** of extracting the bone contours from each of the RF signal **142** is shown. FIG. **10**A illustrates one exemplary, raw RF signal **142** as acquired by one transducer comprising the transducer array **68** (FIG. **2**) of the ultrasound probe portion of the hybrid probe **94** (FIG. **2**). Each acquired raw, RF signal

includes a number of echoes **162**, wherein the echoes **162** may be isolated, partially overlapping, or fully overlapping. Each of the plurality of echoes originates from a reflection of at least a portion of the ultrasound energy at an interface between two tissues having different reflection and/or attenuation coefficients, as described in greater detail below.

[0066] FIGS. **10**B and **10**C illustrate an ultrasound frame **146** having select ones of the raw RF signals **142** with some echoes **162** identified. FIGS. **10**D and **10**E are 3-D renderings of 2D images taken from an ultrasound frame **146** with select ones of the RF signals **142** identified in FIG. **10**E.

[0067] Referring specifically now to FIG. **11**, the method of extracting the bone contour **162***a* begins with a model-based signal processing approach incorporating a priori knowledge of an underlying physical problem into a signal processing scheme. In this way, the computer **54** (FIG. **3**) may process the RF signal **142** and remove some preliminary noise based on an estimated, or anticipated, result. For example, with ultrasound signal acquisition, the physical problem is represented by the governing waveform equation, such as described in VARSLOT T, et al., "Computer Simulation of Forward Wave Propagation in Soft Tissue," *IEEE Transactions on Ultrasonics, Ferroelectrics, and Frequency Control,* 1473-1482:52(9), September 2005, the disclosure of which is incorporated herein by reference, in its entirety. The wave equation describes the propagation behavior of the ultrasonic wave in a heterogeneous medium. The solution to the wave equation may be represented as a state-space model-based processing scheme, such as described in CHEN Z, et al., "Bayesian Filtering: From Kalman Filters to Particle Filters, and Beyond," *Statistics,* 1-69, retrieved from http://citeseerx.ist.psu.edu/viewdoc/download?doi=10.1.1.107.7415&rep=rep1&type=pdf, accessed August 2011. In accordance with one embodiment of the present invention, a general solution to the model-based ultrasound wave estimator problem is developed using Bayesian estimators (e.g., maximum a posteriori), which leads to a nonlinear model-based design.

[0068] The model-based signal processing of the RF signal **142** begins with enhancing the RF signal by applying the model-based signal processing (here, the Bayesian estimator) (Block **167**). To apply the Bayesian estimator, offline measurements are first collected from phantoms, cadavers, and/or simulated tissues to estimate certain unknown parameters, for example, an attenuation coefficient (i.e., absorption and scattering) and an acoustic impedance (i.e., density, porosity, compressibility), in a manner generally described in VARSLOT T (refer above), the disclosure of which is incorporated herein by reference, in its entirety. The offline measurements (Block **169**) are input into the Bayesian estimator and the unknown parameters are estimated as follows:

$$z=h(x)+v \tag{6}$$

$$P(t)=e^{(-\beta t^2)}\cdot\cos(2\pi\cdot f_0\cdot t) \tag{7}$$

Where h is the measurement function that models the system and vis the noise and modeling error. In modeling the system, the parameter, x, that best fits the measurement, z, is determined. For example, the data fitting process may find an estimate of $\hat{x}$ that best fits the measurement of z by minimizing some error norm, $\|\epsilon\|$, of the residual, where:

$$\varepsilon=Z-h(x) \tag{8}$$

[0069] For ultrasound modeling, the input signal, z, is the raw RF signal from the offline measurements, the estimate $h(\hat{x})$ is based on the state space model with known parameters of the offline measurements (i.e., density, etc.). The error, v, may encompass noise, unknown parameters, and modeling errors in an effort to reduce the effect of v by minimizing the residuals and identifying the unknown parameters form repeated measurements. Weighting the last echo within a scan line by approximately 99%, as bone, is one example of using likelihood in a Bayesian framework. A Kalman filter may alternatively be used, which is a special case of the recursive Bayesian estimation, in which the signal is assumed to be linear and have a Gaussian distribution.

[0070] It would be readily appreciated that the illustrative use of the Bayesian model here is not limiting. Rather, other model-based processing algorithms or probabilistic signal processing methods may be used within the spirit of the present invention.

[0071] With the model-based signal processing complete, the RF signal **142** is then transformed into a plurality of envelopes to extract the individual echoes **162** existing in the RF signal **142**. Each envelope is determined by applying a moving power filter to each RF signal **142** (Block **168**) or other suitable envelope detection algorithm. The moving power filter may be comprised of a moving kernel of length that is equal to the average length of an individual ultrasound echo **162**. With each iteration of the moving kernel, the power of the RF signal **142** at the instant kernel position is calculated. One exemplary kernel length may be 20 samples; however, other lengths may also be used. The value of the RF signal **142** represents the value of the signal envelope at that position of the RF signal **142**. Given a discrete-time signal, X having a length, N, each envelope, Y, using a moving power filter having length, L, is defined by:

$$Y_k=\sum_{i=k-\frac{L}{2}}^{k+\frac{L}{2}} X_i^2 \forall\, k\epsilon\left[\frac{L}{2}, N-\frac{L}{2}-1\right] \tag{9}$$

In some embodiments, this and subsequent equations use a one-sided filter of varying length for the special cases of the samples before the L/2 sample (left-sided filter), and after the

$$N-\frac{L}{2}-1$$

sample (right-sided filter).

[0072] Each envelope produced by the moving power filter, shown in FIG. **10**B, includes a plurality of local peaks (identified in FIG. **10**B as enlarged dots at the intersection of each envelope with an echo **162**), each being a clear representation of the individual echoes **162** existing in the acquired RF signal **142** for the various tissue interfaces. As an example of such process, FIGS. **12**A-**12**D more clearly illustrate the RF signal **142** (top in each figure) at four iterations of the kernel of the moving power filter as well as the corresponding envelope (bottom in each figure). Individual echoes **162** in each envelope are again identified with an enlarged dot.

[0073] Of the plurality of echoes **162** in the RF signal **142**, one echo **162** is of particular interest, e.g., the echo corresponding to the bone-soft tissue interface. This bone echo (hereafter referenced as **162***a*) is generated by the reflection of the ultrasound energy at the surface of the scanned bone. More particularly, the soft tissue-bone interface is characterized by a high reflection coefficient of 43%, which means that 43% of the ultrasound energy reaching the surface of the bone is reflected back to the transducer array **68** (FIG. **2**) of the ultrasound probe **60** (FIG. **2**). This high reflectivity gives bone the characteristic hyper-echoic appearance in an ultrasound image.

[0074] Bone is also characterized by a high attenuation coefficient of the applied RF signal (6.9 db/cm/mHz for trabecular bone and 9.94 db/cm/mHz for cortical bone). At high frequencies, such as those used in musculoskeletal imaging (that is, in the range of 7-14 MHz), the attenuation of bone becomes very high and the ultrasound energy ends at the surface of the bone. Therefore, an echo **162***a* corresponding to the soft-tissue-bone interface is the last echo **162***a* in the RF signal **142**. The bone echo **162***a* is identified by selecting the last echo having a normalized envelope amplitude (with respect to a maximum value existing in the envelope) above a preset threshold (Block **170**).

[0075] The bone echoes **162***a* are then extracted from each frame **146** (Block **172**) and used to generate the bone contour existing in that RF signal **142** and as shown in FIG. **100** (Block **174**). In extracting the bone echoes, a probabilistic model (Block **171**) may be input and applied to the RF signals **142** of each frame **146**. The probabilistic model (Block **171**) may further be used in detecting cartilage within the envelopes of the RF signals **142** (Block **173**). While the probabilistic signal processing method may include the Bayesian estimator described previously, in still other embodiments, the signal processing may be, a maximum likelihood ratio, neural network, or a support vector machine ("SVM"), for example, with the latter of which is further described below.

[0076] Prior to implementing the SVM, the SVM may be trained to detect cartilage in RF signals. One such way of training the SVM includes information acquired from a database comprising of MRI images and/or RF ultrasound images to train the SVM to distinguish between echoes associated with cartilage from the RF signals **142**, and from within the noise or in ambiguous soft tissue echoes. In constructing the database in accordance with one embodiment, knee joints from multiple patient's are imaged using both MRI and ultrasound. A volumetric MRI image of each knee joint is reconstructed, processed, and the cartilage and the bone tissues are identified and segmented. The segmented volumetric MRI image is then registered with a corresponding segmented ultrasound image (wherein bone tissue is identified). The registration provides a transformation matrix that may then be used to register the raw RF signals **142** with a reconstructed MRI surface model.

[0077] After the raw RF signals **142** are registered with the reconstructed MRI surface model, spatial information from the volumetric MRI images with respect to the cartilage tissue may be used to determine the location of a cartilage interface on the raw RF signal **142** over the articulating surfaces of the knee joint.

[0078] The database of all knee joint image pairs (MRI and ultrasound) is then used to train the SVM. Generally, the training includes loading all raw RF signals, as well as the location of the bone-cartilage interface of each respective RF signal. The SVM may then determine the location of the cartilage interface in an unknown, input raw RF signal. If desired, a user may chose from one or more kernels to maximize a classification rate of the SVM.

[0079] In use, the trained SVM receives a reconstructed knee joint image of a new patient as well as the raw RF signals. The SVM returns the cartilage location on the RF signal data, which may be used, along with the tracking information from the tracking system (i.e., the optical markers **86** and the position sensor **88** (FIGS. **2**-**2**A) are provided herein) to generate 3-D coordinates for each point on the cartilage interface. The 3-D coordinates may be triangulated and interpolated to form a complete cartilage surface.

[0080] Referring still to FIG. **11**, the resultant bone contours may be noisy and require filtering to remove echoes **162** that may be falsely detected as the bone echo **162***a*. Falsely detected echoes **162** may originate from one of at least two sources: (1) an isolated outlier echoes and (2) a false bone echoes. Furthermore, some images may not include a bone echo **162***a*; therefore any detected echo **162** is noise and should be filtered out. Therefore, proper determination of the preset threshold or filtering algorithm may prevent the false selection of a falsely detected echo **162**.

[0081] Isolated outliers are those echoes **162** in the RF signal **142** that correspond to a tissue interface that is not the soft-tissue-bone interface. Selection of the isolated outliers may occur when the criterion is set too high. If necessary, the isolated outliers may be removed (Block **176**) by applying a median filter to the bone contour. That is, given a particular bone contour, X having a length, N, with a median filter length, L, the median-filter contour, Y_k, is:

$$Y_k = \text{Median}\left[X_{k-\frac{L}{2}}, X_{k+\frac{L}{2}}\right] \forall k \epsilon \left[\frac{L}{2}, N-\frac{L}{2}-1\right] \tag{10}$$

[0082] False bone echoes are those echoes **162** resulting from noise or a scattering echo, which result in a detected bone contour in a position where no bone contour exists. The false bone echoes may occur when an area that does not contain a bone is scanned, the ultrasound probe **60** (FIG. **2**) is not oriented substantially perpendicular with respect to the bone surface, the bone lies deeper than a selected scanning depth, the bone lies within the selected scanning depth but its echo is highly attenuated by the soft tissue overlying the bone, or a combination of the same. Selection of the false bone echoes may occur when the preset threshold is too low.

[0083] Frames **146** containing false bone echoes should be removed. One such method of removing the false bone echoes (Block **178**) may include applying a continuity criteria. That is, because the surface of the bone has a regular shape, the bone contour, in the two-dimensions of the ultrasound image, should be continuous and smooth. A false bone echo will create a non-continuity, and exhibits a high degree of irregularity with respect to the bone contour.

[0084] One manner of filtering out false bone echoes is to apply a moving standard deviation filter; however, other filtering methods may also be used. For example, given the bone contour, X having a length, N, with a median filter length, L, the standard deviation filter contour:

$$Y_k = \sqrt{\frac{1}{L-1}\sum_{i=k-\frac{L}{2}}^{i=k-\frac{L}{2}}(X_i - \overline{X})^2} \;\forall\; k\epsilon\left[\frac{L}{2}, N - \frac{L}{2} - 1\right] \quad (11)$$

Where Y_k is the local standard deviation of the bone contour, which is a measure of the regularity and continuity of the bone contour. Segments of the bone contour including a false bone echo are characterized by a higher degree of irregularity and have a high Y_k value. On the other hand, segments of the bone contour including only echoes resulting from the surface of the bone are characterized by high degree regularity and have a low Y_k value.

[0085] A resultant bone contour **180**, resulting from applying the moving median filter and the moving standard deviation filter, includes a full length contour of the entire surface of the bone, one or more partial contours of the entire surface, or contains no bone contour segments.

[0086] FIGS. **12**A-**12**F and **13**A-**13**F illustrate the resultant bone contour **180** that is selected from those segments of the extracted bone contour that satisfy two conditions: (1) the continuity criteria, having a local standard deviation value below selected standard deviation threshold and (2) a minimum-length criteria, which avoids piecewise-smooth noise contour segments from being falsely detected as bone contour. In some exemplary embodiments, the length of the standard deviation filter may be set to 3 and the threshold set to 1.16 mm, which may correspond to 30 signal samples. Accordingly, FIGS. **13**A and **13**D illustrate two exemplary RF signals **142** with the resultant bone contours **180** extracted and filtered from the noise **182** (including isolated outliers and false body echoes), shown in FIGS. **13**B and **13**E, respectively. FIGS. **13**C and **13**F respectively illustrate the standard deviation, Y_k, calculated as provided in Equation 11 above. FIGS. **14**A-**14**F are similar to FIGS. **13**A-**13**F, but include two exemplary signals **142** in which no bone tissue was scanned.

[0087] With the bone contours isolated from each of the RF signals, the bone contours may now be transformed into a point cloud. For instance, returning now to FIG. **7**, the resultant bone contours **180** may then undergo registration with the optical system to construct a bone point cloud **194** representing the surface of at least a portion of each scanned bone (Block **186**), which is described herein as a multiple step registration process. In one embodiment, the process is a two-step registration process. The registration step (Block **186**) begins by transforming the resultant bone contour **180** from a 2D contour in the ultrasound frame into a 3-D contour in the world frame (Block **188**). This transformation is applied to all resultant bone contours **180** extracted from all of the acquired RF signals **142**.

[0088] To transform the resultant bone contour **180** into the 3-D contour, each detected bone echo **162***a* undergoes transformation into a 3-D point as follows:

$$d_{echo} = n_{echo} T_s C_{us} \quad (12)$$

$$l_{echo} = L_{trans}\frac{n_{line}}{N_{lines}}\hat{u}_x \quad (13)$$

$$P_{echo}^{OP} = P_{trans-origin} + d_{echo}\hat{u}_y + l_{echo}\hat{u}_x \quad (14)$$

-continued

$$P_{echo}^{W} = H_{OP}^{W} P_{echo}^{OP} \quad (15)$$

Where the variables are defined as follows:

d_{echo}	depth of the bone echo (cm)
n_{echo}	sample index of the detected bone echo
T_s	RF signal sampling period (sec/sample)
C_{us}	speed of ultrasound in soft tissue (154×10^3 cm/s)
l_{echo}	distance from the $P_{trans-origin}$ (FIG. 2) of the transducer array 68 (FIG. 2) to the current scan line (cm)
P_{echo}^{OP}	detected point on the bone surface represented in the local frame
n_{line}	index of the scan line containing the bone echo in the image
N_{lines}	number of scan lines in the image
P_{echo}^{W}	detected surface of the bone relative to the world frame
H_{OP}^{W}	homogeneous transformation between the local frame and the world frame, as described previously
H_{OP}^{W}	dynamically obtained transformation that contains the position and orientation of the optical marker 86 (FIG. 2)

[0089] If so desired, an intermediate registration process may be performed between the resultant bone contour and a B-mode image, if acquired (Block **190**). This registration step is performed for visualizing the resultant bone contour **180** with the B-mode image (FIG. **9**), which provides visual validation and feedback of the resultant bone contour **180** detection process, in real time, while the user is performing the scan. This visual validation may aid the user in determining whether acquisition is completed (Block **160**), as described previously. More specifically, the resultant bone contour **180** is registered with the B-mode image by:

$$P_{echo}^{I} = (l_{echo} I_x d_{echo} I_y) \quad (16)$$

Where I_x and I_y denote the B-mode image resolution (pixels/cm) for the x- and y-axes respectively. P_{echo}^{I} denotes the coordinates of the bone contour point relative to the ultrasound frame.

[0090] After the resultant bone contours **180** are transformed and, if desired, registered (Block **190**) (FIG. **15**), the plurality of point clouds **165** (FIG. **16**B) are generated representing the surface of the bone. During the second registration process the plurality of point clouds **165** are integrated into a bone point cloud **194** representing the entire surface of the scanned bone.

[0091] To begin the second registration process, as shown in FIGS. **16**A-**17**D, the plurality of point clouds **164** are initially aligned to a standardized model of the scanned bone, here a model femur **200**, for example, by using 4-6 previously specified landmarks **196** (Block **192**). More specifically, the user may identify the plurality of landmarks **196** on the model femur **200**, which need not be identified with high accuracy. After this initial alignment, an iterative closest point ("ICP") alignment is performed to more accurately align the plurality of point clouds to the standardized model. If necessary, noise may be removed by thresholding for a distance between a respective point of the plurality of point clouds and the closest vertices in the model femur **200**; however, other filtering methods may alternatively be used. For instance, an average distance plus one standard deviation may be used as the threshold. The process is repeated for each point cloud **165** of the plurality for the surface of the scanned bone.

[0092] The now aligned point clouds **165** are then integrated into a single uniform point cloud **194** that represents the surface of the scanned bone (Block **202**).

[0093] After the point clouds **194** are formed, a bone model may be optimized in accordance with the point clouds **194**. That is, the bone point cloud **194** is then used to reconstruct a 3-D patient-specific model of the surface of the scanned bone. The reconstruction begins with a determination of a bone model from which the 3-D patient-specific model is derived (Block **210**). The bone model may be a generalized model based on multiple patient bone models and may be selected from a principle component analysis ("PCA") based statistical bone atlas. One such a priori bone atlas, formed in accordance with the method **212** of FIG. **18**, includes a dataset of 400 dry femur and tibia bone pairs, scanned by CT (Block **214**) and segmented to create models of each bone (Block **216**). The method of building and using one such statistical atlas is described in MAHFOUZ M et al., "Automatic Methods for Characterization of Sexual Dimorphism of Adult Femora: Distal Femur," *Computer Methods in Biomechanics and Biomedical Engineering*, 10(6) 2007, the disclosure of which is incorporated herein by reference in its entirety.

[0094] Each bone model, M_i, (where I∈[1, N], N being the number of models in the dataset) has the same number of vertices, wherein the vertex, V_j in a select one model corresponds (at the same anatomical location on the bone) to the vertex, V_j in another one model within the statistical atlas.

[0095] PCA was then performed on each model in the dataset to extract the modes of variation of the surface of the bone (Block **218**). Each mode of variation is represented by a plurality of eigenvectors resulting from the PCA. The eigenvectors, sometimes called eigenbones, define a vector space of bone morphology variations extracted from the dataset. The PCA may include any one model from the dataset, expressed as a linear combination of the eigenbones. An average model of all of the 3-D models comprising the dataset is extracted (Block **220**) and may be defined as:

$$M_{avg} = \frac{1}{N}\sum_{i=1}^{N} M_i \tag{17}$$

$$M_i = M_{avg} + E_{k=1}^{L}\alpha_{ik} U_k \quad \forall i\epsilon[1, N] \tag{18}$$

Where the variables are defined as follows:

M_{avg}	is the mean bone of the dataset
L	dimensionality of the eigenspace (i.e., the number of eigenbones) and is equal to N
N	number of models in the data
U_k	k^{th} eigenbone
α_{ik}	k^{th} shape descriptor or eigenbone's coefficient for the i^{th} model

[0096] Furthermore, any new model, M_{new}, i.e., a model not already existing in the dataset, may be approximately represented by new values of the shape descriptors (eigenvectors coefficients) as follows:

$$M_{new} \cong M_{avg} + \Sigma_{k=1}^{W}\alpha_k U_k \tag{19}$$

Where the variables are defined as follows:

M_{new}	new bone model
α_k	indexed shape descriptors for the new model
W	number of principal components to use in the model approximation, where W ≤ L

[0097] The accuracy of M_{new} is directly proportional to the number of principal components (W) used in approximating the new model and the number of models, L, of the dataset used for the PCA. The residual error or root mean square error ("RMS") for using the PCA shape descriptors is defined by:

$$\text{RMS} = \text{rms}[M_{new} - (M_{avg} + \Sigma_{k=1}^{W}\alpha_k U_k)] \tag{20}$$

[0098] Therefore, the RMS when comparing any two different models, A and B, having the same number of vertices is defined by:

$$\text{RMS} = \text{rms}(A - B) = \sqrt{\frac{\sum_{j=1}^{m} \|V_{Aj} - V_{Bj}\|^2}{m}} \tag{21}$$

Where V_{Aj} is the j^{th} vertex in model A, and similarly, V_{Bj} is the j^{th} vertex in model B.

[0099] Returning again to FIG. **7**, the average model ("AVERAGE" branch of Block **210**) is loaded (Block **230**) or a subset model is selected ("SELECTED" branch of Block **210**) from the statistical atlas based on demographics that are similar to the patient and loaded (Block **232**) for optimization. The bone point cloud **194** is then applied to the loaded model (Block **234**) so that the shape descriptors of the loaded model may be changed to create the 3-D patient-specific model. If desired, one or more shape descriptors may be constrained ("YES" branch of Block **254**) so that the 3-D patient-specific model will have the same anatomical characteristics as the loaded model. Accordingly, the one or more shape descriptors are set (Block **238**). With the constraints set, the loaded model may be deformed (or optimized) (Block **240**) into a model that resembles the appropriate bone and not an irregularly, randomly shaped model. If no constraints are desired ("NO" branch of Block **240**) and then the loaded model is optimized (Block **240**).

[0100] Changing the shape descriptors to optimize the loaded model (Block **240**) may be carried out by one or more optimization algorithms, guided by a scoring function, to find the values of the principal components coefficients to create the 3-D patient-specific new model and are described with reference to FIG. **19**. The illustrated optimization algorithm includes a two-step optimization method of successively-applied algorithms to obtain the 3-D patient-specific model that best fits the bone point cloud **194** as discussed below. Although a two-step method is described, the present invention is not limited to just a two-step optimization method.

[0101] The first algorithm may use a numerical method of searching the eigenspace for optimal shape descriptors. More specifically, the first algorithm may be an iterative method that searches the shape descriptors of the loaded model to find a point that best matches the bone point cloud **194** (Block **250**). One such iterative method may include, for example, Powell's conjugate gradient descent method with a RMS as the scoring function. The changes are applied to

the shape descriptors of the loaded model by the first algorithm to form a new model, M_{new}, (Block **252**) defined by Equation 19. The new model, M_{new}, is then compared with the bone point cloud **194** and the residual error, E, calculated to determine whether a further iterative search is required (Block **254**). More specifically, given a bone point cloud, Q, having n points therein, and an average model, M_{avg}, with I vertices, there may be a set of closest vertices, V in the average model, M_{avg} to the bone point cloud, Q.

$$v_i = arg\min_{v_j \in M} \|v_j - q_i\| \forall i \in [1,n], j \in [1,I] \tag{22}$$

Where v_i is the closest point in the set, V, to q_i in the bone point cloud, Q. An octreemay be used to efficiently search for the closest points in M_{new}. The residual error, E, between the new model, M_{new} and the bone point cloud, Q, is then defined as:

$$E = \|V - Q\|^2 \tag{23}$$

[0102] With sufficiently high residual error ("YES" branch of Block **254**), the method returns to further search the shape descriptors (Block **250**). If the residual error is low ("NO" branch of Block **254**), then the method proceeds.

[0103] The second algorithm of the two-step method refines the new model derived from the first algorithm by transforming the new model into a linear system of equations in the shape descriptors. The linear system is easily solved by linear system equation, implementing conventional solving techniques, which provide the 3-D patient-specific shape descriptors.

[0104] In continuing with FIG. **19**, and to transform the new model into the linear system, the roots of the linear system must be determined (Block **256**). More specifically, the first partial derivatives of the residual error, E, with respect to the shape descriptors, α_k, are equal to zero. The error function, Equation 23, may be expressed in terms of the vertices, v_i, of the set, V, and the points, p_i, of the point cloud, Q:

$$E = \Sigma_{i=1}^{m} \|v_i - q_i\|^2 \tag{24}$$

And may also be expressed in terms of the new model's shape descriptors as:

$$E = \|(V_{avg} + \Sigma_{k=1}^{W} a_k U'_k) - Q\|^2 \tag{25}$$

Where V_{avg} is the set of vertices from the loaded model's vertices, which corresponds to the vertices set, V, that contains the closest vertices in the new model, M_{new}, that is being morphed to fit the bone point cloud, Q. U'_k is a reduced version of the k^{th} eigenbone, U_k, containing only the set of vertices corresponding to the vertices set, V.

[0105] Combining Equations 24 and 25, E maybe expressed as:

$$E = \Sigma_{i=1}^{m} \|(v_{avg,i} + \Sigma_{k=1}^{w} a_k u'_{k,i}) - q_i\|^2 \tag{26}$$

Where $v_{avg,i}$ is the i^{th} vertex of V_{avg}. Similarly, $u'_{k,i}$ is the i^{th} vertex of the reduced eigenbone, U'_k.

[0106] The error function may be expanded as:

$$E = \Sigma_{i=1}^{m} [(x_{avg,i} + \Sigma_{l=1}^{W} a_k x_{u',l,i} - x_{q,i})^2 + (y_{avg,i} + \Sigma_{l=1}^{W} a_k y_{u',l,i} - y_{q,i})^2 + (z_{avg,i} + \Sigma_{l=1}^{W} a_k z_{u',l,i} - z_{q,i})^2] \tag{27}$$

Where $x_{avg,i}$ is the x-coordinate of the i^{th} vertex of the average model, $x_{k,i}$ is the x-coordinate of the i^{th} vertex of the k^{th} eigenbone, and $x_{Q,i}$ is the x-coordinate of the i^{th} point of the point cloud, Q. Similar arguments are applied to the y- and z-coordinates. Calculating the partial derivative of E with respect to each shape descriptor, α_k, yields:

$$\frac{\partial E}{\partial \alpha_k} = 0 \ \forall k \in [1, W] \tag{28}$$

$$\frac{\partial E}{\partial \alpha_k} = \sum_{i=1}^{m} \left[2\left(x_{avg,i} + \sum_{l=1}^{W} a_l x_{u',l,} - x_{p,i}\right) + 2\left(y_{avg,i} + \sum_{l=1}^{W} a_l y_{u',l,i} - y_{p,i}\right) y_{k,i} + 2\left(z_{avg,i} + \sum_{l=1}^{W} a_k z_{u',l,i} - z_{p,i}\right) z_{k,i}\right] = 0 \ \forall k \in [1, W] \tag{29}$$

[0107] Recombining the coordinate values into vectors yields:

$$\frac{\partial E}{\partial \alpha_k} = \sum_{i=1}^{m} \left[(v_{avg,i} \cdot u'_{k,i}) + \left(\sum_{l=1}^{W} a_l u'_{l,i}\right) \cdot u'_{k,i} - q_i \cdot u'_{k,i}\right] = 0 \ \forall k \in [1, W] \tag{30}$$

And with rearrangement:

$$\Sigma_{i=1}^{m} (\Sigma_{l=1}^{w} a_l (u'_{l,i} \cdot u'_{k,i})) = \Sigma_{i=1}^{m} [q_i \cdot u'_{k,i} - (v_{avg,i} \cdot u'_{k,i})] \tag{31}$$

[0108] Reformulating Equation 31 into a matrix form provides a linear system of equations in the form of Ax=B:

$$\sum_{i=1}^{m} \begin{bmatrix} u'_{1,i} \cdot u'_{1,i} & u'_{2,i} \cdot u'_{1,i} & \cdots & \cdots & u'_{W,i} \cdot u'_{1,i} \\ u'_{1,i} \cdot u'_{2,i} & u'_{2,i} \cdot u'_{2,i} & \cdots & \cdots & u'_{W,i} \cdot u'_{2,i} \\ \vdots & \vdots & \ddots & \ddots & \vdots \\ \vdots & \vdots & \ddots & \ddots & \vdots \\ u'_{1,i} \cdot u'_{W,i} & u'_{2,i} \cdot u'_{W,i} & \cdots & \cdots & u'_{W,i} \cdot u'_{W,i} \end{bmatrix} \begin{bmatrix} a_1 \\ a_2 \\ \vdots \\ \vdots \\ a_W \end{bmatrix} = \sum_{i=1}^{m} \begin{bmatrix} (q_i - v_{avg,i}) \cdot u'_{1,i}) \\ (q_i - v_{avg,i}) \cdot u'_{2,i}) \\ \vdots \\ \vdots \\ (q_i - v_{avg,i}) \cdot u'_{W,i}) \end{bmatrix} \tag{32}$$

[0109] The linear system of equations may be solved using any number of known methods, for instance, singular value decomposition (Block **258**).

[0110] In one embodiment, the mahalanobis distance is omitted because the bone point clouds are dense, thus providing a constraining force on the model deformation. Therefore the constraining function of the mahalanobis distance may not be needed, but rather was avoided to provide the model deformation with more freedom to generate a new model that best fit the bone point cloud.

[0111] An ultrasound procedure in accordance with the embodiments of the present invention may, for example, generate approximately 5000 ultrasound images. The generated 3-D patient-specific models (Block **260**, FIG. **7**), when compared against CT-based segmented models, yielded an average error of approximately 2 mm.

[0112] The solution to the linear set of equations provides a description of the patient-specific 3-D model, derived from an average, or select model, from the statistical atlas, and optimized in accordance with the point cloud transformed from a bone contour that was isolated from a plurality of RF signals. The solution may be applied to the average model to display a patient-specific 3-D bone model for aiding in

pre-operative planning, mapping out injection points, planning a physical therapy regiment, or other diagnostic and/or treatment-based procedure that involves a portion of the musculoskeletal system.

[0113] Cartilage 3-D models may be reconstructed a method that is similar to that which was outlined above for bone. During contour extraction, the contour of the cartilage is more difficult to detect than bone. Probabilistic modeling (Block **171**) is used to process the raw RF signal to more easily identify cartilage, and SVM aids in detection of cartilage boundaries (Block **173**) based on MRI training sets. A cartilage statistical atlas is formed by a method that may be similar to what was described for bone; however, as indicated previously, MRI is used rather than the CT (which was the case for bone). The segmentation (Block **216**), variation extraction (Block **218**) and base model morphing (Block **240**) (FIG. **19**) are processed to produce a reconstructed cartilage model in the same manner as a bone model is reconstructed. The cartilage model may be displayed alone, or in conjunction with the 3D patient-specific bone model.

[0114] While the present invention has been illustrated by the description of the embodiments thereof, and while the embodiments have been described in considerable detail, it is not the intention of the applicant to restrict or in any way limit the scope of the appended claims to such detail. Additional advantages and modifications will readily appear to those skilled in the art. Therefore, the present invention in its broader aspects is not limited to the specific details representative apparatus and method, and illustrative examples shown and described. Accordingly, departures may be made from such details without departure from the spirit or scope of applicant's general inventive concept.

1.-**32**. (canceled)

33. A method of generating a virtual three dimensional subject-specific musculoskeletal model, the method comprising:

generating an envelope for each of a plurality of raw signals obtained from an ultrasound scan of at least a portion of a subject, each envelope including one or more peaks;

generating contour lines based on the peaks of the envelopes;

transforming the contour lines into a three dimensional (3-D) point cloud using tracking information obtained by tracking a position of an ultrasound transducer during the ultrasound scan of at least the portion of the subject; and

optimizing a template tissue model with respect to the point cloud to generate a virtual three dimensional subject-specific musculoskeletal model.

34. The method according to claim **33**, wherein the plurality of raw signals includes a first raw signal at a first frequency and a second raw signal at a second frequency, where the first frequency is different than the second frequency.

35. The method according to claim **33**, further comprising:

transmitting ultrasound signals during the ultrasound scan; and

obtaining the plurality of raw signals responsive to transmitting the ultrasound signals.

36. The method according to claim **35**, wherein obtaining the plurality of raw signals comprises:

receiving reflected ultrasound energy from each of the transmitted ultrasound signals; and,

converting the reflected ultrasound energy from each of the transmitted ultrasound signals into the plurality of raw signals.

37. The method according to claim **35**, wherein transmitting the ultrasound signals comprises:

transmitting a plurality of ultrasound pulses each having a frequency; and,

changing the frequency of the ultrasound pulses as the raw signals are acquired.

38. The method according to claim **37**, wherein the frequency of the ultrasound pulses is changed by sweeping the frequency.

39. The method of claim **33**, wherein generating the contour lines based on the peaks of the envelope signals comprises:

identifying a first peak of the one or more peaks in each envelope; and

applying a first filter to the first peaks in temporally adjacent envelopes.

40. The method according to claim **39**, wherein the first peak is identified in each of the envelopes by using a second filter to estimate an optimal time delay.

41. The method according to claim **40**, wherein the second filter is selected from a group consisting of a Kalman filter, a recursive Bayesian filter, and a particles filter.

42. The method according to claim **39**, wherein the first filter is based on Bayesian model smoothing.

43. The method according to claim **33**, wherein generating the contour lines based on the peaks of the envelopes comprises:

calculating a first peak data matrix for the envelope of a first raw signal of the plurality of raw signals;

estimating a second peak data matrix for the envelope of a second raw signal of the plurality of raw signals based on the first peak data matrix;

calculating the second peak data matrix from the envelope of the second raw signal;

calculating an error matrix based on a difference between the estimated second peak data matrix and the calculated second peak data matrix; and

calculating an error correction gain based on the error matrix.

44. The method according to claim **43**, further comprising estimating a third peak data matrix for the envelope of a third raw signal of the plurality of raw signals by multiplying the error matrix by the error correction gain, and adding a product of the multiplication to the calculated second peak data matrix.

45. The method according to claim **33**, wherein generating the contour lines based on the peaks of the envelopes comprises:

calculating a first peak data matrix for the envelope of a first raw signal of the plurality of raw signals;

generating a first set of particles for each peak in the first peak data matrix;

estimating a second peak data matrix for the envelope of a second raw signal of the plurality of raw signals based on the first set of particles for each peak in the first peak data matrix;

calculating a second peak data matrix for the envelope of the second raw signal;

calculating an error matrix based on a difference between the estimated second peak data matrix and the calculated second peak data matrix;

generating a second set of particles for each peak in the second peak data matrix; and

calculating a weight for each particle in the second set of particles for each peak in the second peak data matrix based on the error matrix.

46. The method according to claim **45**, comprising estimating a third peak data matrix for the envelope of a third raw signal of the plurality of raw signals based on the weighted particles of the second set of particles for each peak in the second peak data matrix.

47. The method according to claim **44**, wherein the first raw signal, the second raw signal, and the third raw signal are temporally adjacent raw signals.

48. The method according to claim **33**, wherein transforming the contour lines into the 3-D point cloud includes extracting a 2-D feature from each contour line.

49. The method according to claim **33**, wherein the contour lines are generated by:

applying a statistical weight to each of the one or more peaks in each of the envelopes to create weighted peaks; and

determining a path of each of the contour lines across the envelopes based on the weighted peaks.

50. An apparatus for generating a 3-D subject-specific musculoskeletal model, the apparatus comprising:

a processor; and

a memory containing instructions that, when executed by the processor, cause the apparatus to:

generate an envelope for each of a plurality of raw signals obtained from an ultrasound scan of at least a portion of a subject, each envelope including one or more peaks;

generate contour lines based on the peaks of the envelopes;

transform the contour lines into a three dimensional (3-D) point cloud using tracking information obtained by tracking a position of an ultrasound transducer during the ultrasound scan of at least the portion of the subject; and

optimize a template tissue model with respect to the point cloud to generate a virtual three dimensional subject-specific musculoskeletal model.

* * * * *

专利名称(译)	超声三维重建关节的方法和设备		
公开(公告)号	US20200000436A1	公开(公告)日	2020-01-02
申请号	US16/567873	申请日	2019-09-11
[标]申请(专利权)人(译)	JOINTVUE		
申请(专利权)人(译)	JOINTVUE，LLC		
当前申请(专利权)人(译)	JOINTVUE，LLC		
[标]发明人	MAHFOUZ MOHAMED R		
发明人	MAHFOUZ, MOHAMED R.		
IPC分类号	A61B8/08 A61B8/00 G06T17/00		
CPC分类号	A61B8/0875 A61B8/5207 A61B8/14 A61B8/4405 A61B8/466 G06T2210/41 G06T7/564 G06T17/00 A61B5/0035 A61B5/055 A61B5/4504 A61B8/4245 A61B8/4263 A61B8/483 A61B8/5246 A61B34/10 A61B2034/105 A61B2034/2055 A61B2090/367 A61B2090/378 G06T19/20 G06T2210/56 G06T2219/2021		
优先权	61/470952 2011-04-01 US 61/369848 2010-08-02 US		
外部链接	Espacenet USPTO		

摘要(译)

一种生成3-D患者特定骨骼模型的方法，该方法包括：（a）使用多个位置的患者骨骼的A模式超声扫描获取多个原始射频（RF）信号 超声探头，其包括换能器阵列；（b）跟踪3-D空间中多个原始RF信号的获取并生成相应的跟踪数据；（c）通过对多个原始RF信号的每一个应用包络线检测算法，将多个原始RF信号的每一个变换为包括多个峰的包络，每个峰值对应于组织界面回波；（d）通过选择具有高于预设阈值的归一化包络幅度的最后一个峰值，从多个原始RF信号中的每一个的组织界面回波中识别出骨回波以包括多个骨回波，其中，将包络幅度用 关于包络中存在的最大峰值；（e）从对应于超声探头的每个位置的多个骨回波中确定2-D骨轮廓，以包括2-D骨轮廓；（f）使用跟踪数据将2D骨骼轮廓转换为集成的3D点云；（g）使与患者的骨骼相对应的非患者特定的3-D骨骼模型对应于集成的3-D点云变形以生成3-D患者特定的骨骼模型。